공학석사학위 논문

Improvement of Cycle Life for Both Cathode and Anode through Tris(pentafluorophenyl)silane Electrolyte Additive

Tris(pentafluorophenyl)silane 전해질 첨가제를 통한 양극과 음극의 수명 특성 향상

2014년 2월

서울대학교 대학원

화학생물공학부

이태진

Improvement of Cycle Life for Both Cathode and Anode through Tris(pentafluorophenyl)silane Electrolyte Additive

지도교수 오 승 모

이 논문을 공학석사 학위논문으로 제출함

2013년 12월

서울대학교 대학원

화학생물공학부

이 태 진

이태진의 공학석사학위 논문을 인준함

2014년 2월

위 원 장 김 영 규 (인)

부위원장 오 승 모 (인)

위 원 김 상 기 (인)

Abstract

Since lithium ion battery is commercialized, it has been expanding its application from IT mobile device to EV. This tendency is demanding much higher energy density of lithium ion battery. Higher energy density strategy is classified into 2 methods. They are increasing capacity and increasing voltage. Voltage increase is reviewed by so many researchers. To do this, it uses high voltage cathode materials without changing the existing low voltage anode.

There is a barrier to apply for high voltage cathode materials, it is electrolyte oxidation. And also, it is still remained reductive stability of electrolyte, which has been a problem. So, it is necessary to jump out these problems. To overcome this obstacle, it is most favorable to use electrolyte additive. So many additives are reported to effect on graphite, but few additives are reported to effect on high voltage cathode materials. For example, VC additive shows very good performance on graphite, but it could be applied to high voltage cathode any more due to oxidation stability. So, there is a need to develop additive for high voltage cathode materials and it showed good effect on low voltage anode like graphite.

So, this research is to develop electrolyte additive for both cathode and anode. TPFPS showed good cycle performance and coulombic efficiency than additive-free electrolyte. This effect is confirmed by EIS, XPS spectra. Film resistance mitigation is the main factor of TPFPS effects during cycling. It was confirmed by XPS data, through film thickness of $LiNi_{0.5}Mn_{1.5}O_4$, and inorganic component of anode each.

List of Figures

Figure 31. FE-SEM images were obtained from 100th lithiation step. (a) pristine electrode, (b) SEI of additive-free electrolyte, and (c) SEI of TPFPS after cycling.

List of Table

Contents

1. Introduction

Since lithium-ion battery is commercialized by SONY in 1992, it has been used power sources in mobile device like cell phone, digital camera, notebook, tablet PC. Now, we expect that it could be applied to EV, hybrid vehicle, ESS(Energy storage system) beyond these IT applications. Therefore, we have been asked to develop to increase high energy density cell. Energy is capacity multiplication voltage. To increase high energy density, there are two methods, 1st one is increasing capacity, the other one is increasing operation voltage.

Among these methods, research trend of increasing cell voltage has been progressing. Cell voltage is determined by the difference between cathode and anode. But, lowering anode operation voltage (*vs.* Li/Li^+) would be very difficult, because no materials lower than Li metal(Li/Li^+ redox reaction) have been in earth. So, raising cathode operation voltage has been studying these days.

There are barriers for commercializing high-voltage cathode materials, though these materials have been already developed. This is because of the electrochemical oxidation and reduction stability of commercialized electrolytes. If we use high-voltage advantage, the low voltage anode commercialized like graphite must be remained in lithium ion battery, and the high-voltage materials should be applied in the system. The electrochemical reduction stability of electrolytes has been already issued in anode, now we will be faced with the electrochemical oxidation stability of electrolytes. According to Goodenough, the following Figure 1, the electrochemical stability

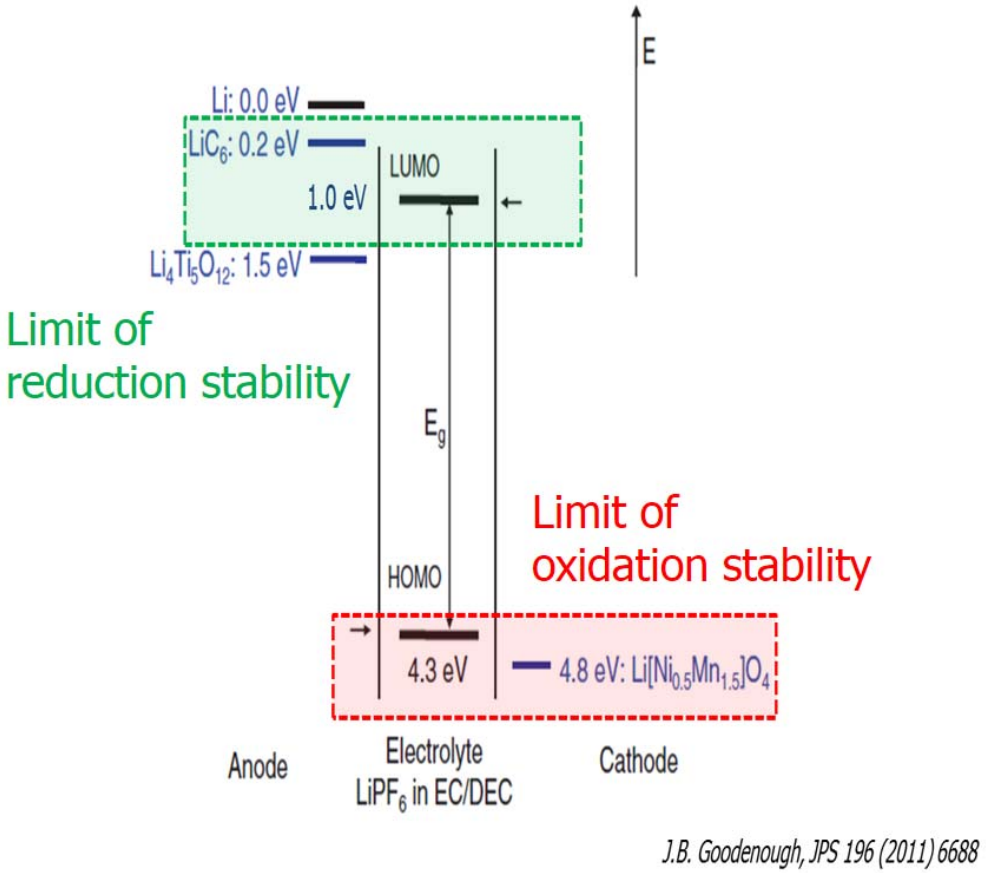

Figure 1. Electrochemical stability window

window of electrolytes, the limit of reduction is 1.0V(*vs.* Li/Li+) and the limit of oxidation is 4.3V(*vs.* Li/Li+).[1]

Therefore, the commercialized anode and the high-voltage cathode materials are operated beyond the electrochemical stability window. As a results, the electrolyte decomposed products are formed on active materials in these situations.(Figure 2.) These products are accumulated in the form of surface film. Peled named it SEI(Solid Electrolyte Interphase) about anode[2], because this layer is between electrolyte solution and negative electrode and plays a role in Li^+ diffusion path. If SEI formed in initial cycling can't prevent further electrolyte decomposition, these accumulated SEI products would be one factor of internal cell resistance. The larger internal cell resistance, the more cell capacity decrease from an iR drop perspective. Also, this phenomena occurs in positive electrode.

There are blocking ways of these side reaction of electrolyte. 1st one is alternative electrolyte like ionic liquid, and polymer electrolyte. 2nd one is coating of active materials. The last one is using electrolyte additive. This method is the strategy to form different surface film on active materials during pre-cycling. In initial cycling, the electrolyte additives decompose to form different surface film sacrificially. Among these method, electrolyte additive is the best, because no need to change the established electrolyte, and cost advantage due to small amount of its quantity.

On the other hand, a lot of additives effective on negative electrode has been already developed like VC(Vinylene carbonate)[3]. But, the additives effective on positive

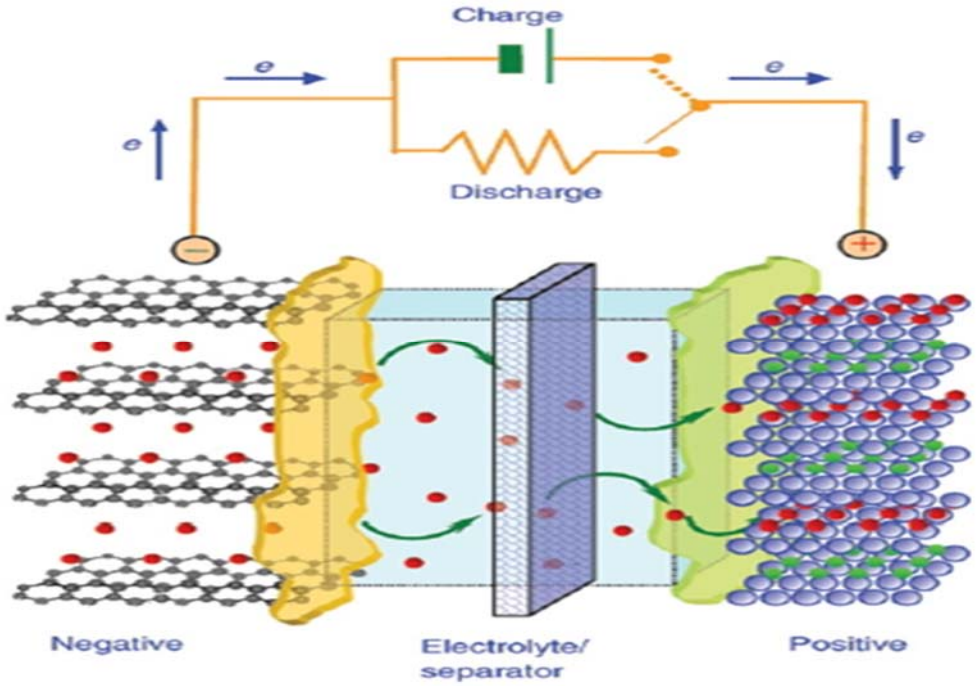

Figure 2. SEI or film layer is formed on both negative and positive electrode surface attributed to electrolyte stability windows.

electrode has not been developed recently. So, we need to develop the electrolyte additive for positive electrode.

This study is to develop the electrolyte additive for both cathode and anode materials. If we solve electrolyte reduction and oxidation problems at the same time, it would be more valuable research. Because electrolyte additives developed recently are hardly effective on both negative and positive electrode simultaneously. For example, the famous additive, VC could not applied to high-voltage cathode materials due to electrochemical oxidative instability.[4]

In this study, Figure 3, tris(pentafluorophenyl)silane(below TPFPS) is used as additive. According to previous report[5, 6], the similar chemical structure, tris(pentafluorophenyl)borane and tris(pentafluorophenyl)phosphine showed good cycle performance on cathode and anode each electrode. The electron cloud distribution of these structures is that the center atom is electron deficient and outer fluorine is very electron withdrawing atom. Because reduction and oxidation voltage of additive correlates with its HOMO/LUJMO energy level, we can expect tris(pentafluorophenyl)silane would be effective on both cathode and anode, too. In these articles, these additives decompose on each electrode sacrificially to make different SEI or passivation layer. By using TPFPS as electrolyte additive, it was found that improvement of cycle life and coulombic efficiency for both $LiNi_{0.5}Mn_{1.5}O_4$ cathode material and graphite anode.

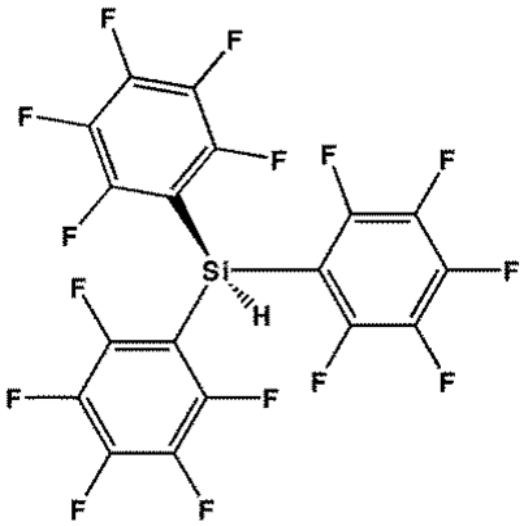

Figure 3. Tris(pentafluorophenyl)silane.

2. Background for Lithium ion battery

2.1. Cathode material – $LiNi_{0.5}Mn_{1.5}O_4$

$LiNi_{0.5}Mn_{1.5}O_4$ is high voltage cathode material. Figure 4, it is composed of two structures of spinel, $Fd\bar{3}m$ and $P4_332$. $Fd\bar{3}m$, face-centered spinel, is caused from Mn^{3+} impurity, and $P4_332$, ordered spinel, is originated from Mn^{4+} construction ion of $LiNi_{0.5}Mn_{1.5}O_4$ spinel structure[7]. According to temperature, only $P4_332$ structure is possible to synthesized. But, it was known that $LiNi_{0.5}Mn_{1.5}O_4$ mixed with small quantity of Mn^{3+} have showed more higher cycle performance than $LiNi_{0.5}Mn_{1.5}O_4$ added no Mn^{3+}.

On the other hand, the reaction voltage and capacity of $LiNi_{0.5}Mn_{1.5}O_4$are related with Ni^{2+} ion. The reaction mechanism of $LiNi_{0.5}Mn_{1.5}O_4$ is oxidation number change of Ni^{2+}. During charging, Ni^{2+} oxidizes 2 times and releases 2 electrons. In discharging, the reverse reaction occurs[8]. So, capacity of $LiNi_{0.5}Mn_{1.5}O_4$ is the electron release quantity of Ni^{2+} ion. The theoretical capacity of $LiNi_{0.5}Mn_{1.5}O_4$ is 147.7 mA h g^{-1}, and the practical capacity of $LiNi_{0.5}Mn_{1.5}O_4$ is 120 mA h g^{-1}.

$$Ni^{2+} \rightleftharpoons Ni^{3+} + e^- \rightleftharpoons Ni^{4+} + e^-$$

$$LiNi_{0.5}Mn_{1.5}O_4 \rightleftharpoons Ni_{0.5}Mn_{1.5}O_4 + Li^+ + e^-$$

The reaction voltage is associated with Figure. 5 Ni^{2+} electron energy state. It is high voltage cathode material and was originally the substitution from Mn^{3+} to Ni^{2+} of

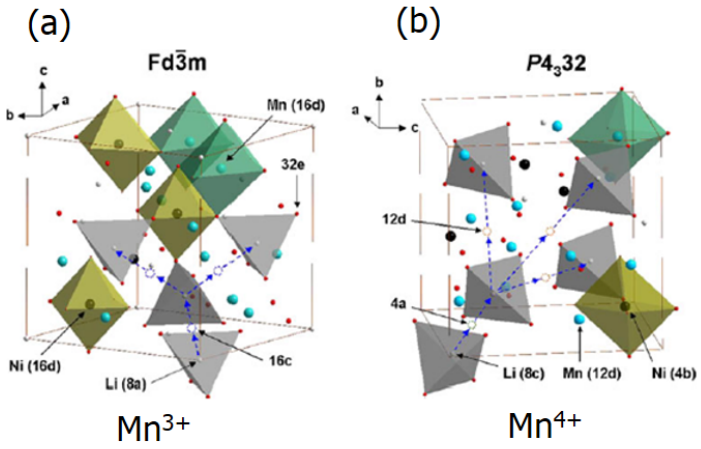

Figure 4. $LiNi_{0.5}Mn_{1.5}O_4$ is composed of two spinel structure (a) $Fd\bar{3}m$ (b) $P4_332$

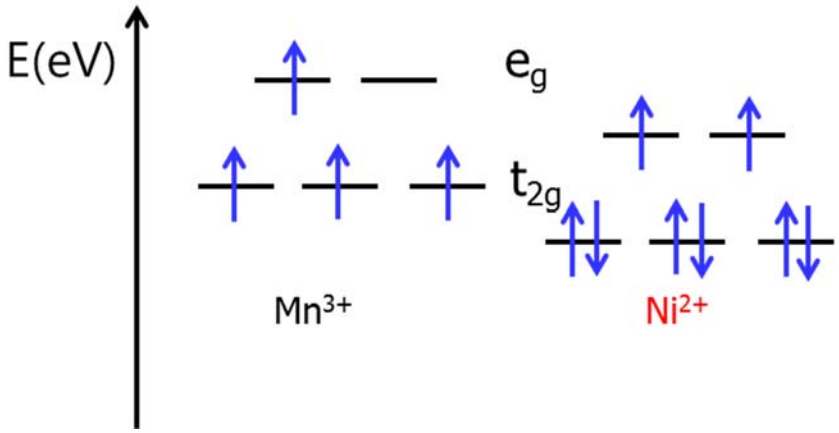

Figure 5. Electronic energy states, Mn^{3+} of $LiMn_2O_4$ and Ni^{2+} of $LiNi_{0.5}Mn_{1.5}O_4$

$LiMn_2O_4$. Theoretically, oxidation of Mn^{4+} ion can not be occurred. Eg electron energy level of Ni^{2+} locates lower than Mn^{3+} of $LiMn_2O_4$, so it has more stable HOMO electron energy level. Because the more stable HOMO level, the higher reaction voltage, the Ni^{2+} reaction voltage, ~4.75V(*vs.* Li/Li^+) of $LiNi_{0.5}Mn_{1.5}O_4$ is higher than ~4V(*vs.* Li/Li^+) Mn^{3+} reaction voltage.

2.2. Anode material – Natural graphite

Graphite is stacked in ABAB sequence of graphene layer through z-axis direction. Its structure (Figure 6.) is mainly hexagonal structure[9], but some graphite involves rhombohedra graphite.

The reaction mechanism with Li^+ is following that and it occurs below 0.25 V (*vs.* Li/Li^+)

$$C + {}_xLi \rightleftharpoons Li_xC \qquad (< 0.25\ \text{V vs. Li / Li}^+)$$

Theoretical capacity, the maximum of Li+ amounts that could be inserted, is 372 mA h g^{-1}. Practical capacity is about 360 mA h g^{-1} in case of natural graphite and about 320 mA h g^{-1} in case of artificial graphite.

Li^+ reaction aspects of graphite showed 3 plateau in their voltage profile. When Li^+ reactions, it is inserted in space of graphene layers. But, Li^+ insertion could not be occurred from 1st floor to highest floor. Because, if it occurs, repulsive interaction of graphene layer is so strong, and it is in very unstable energy state. So, Li^+ is inserted between gap of graphene layers with some intervals. This phenomenon is called

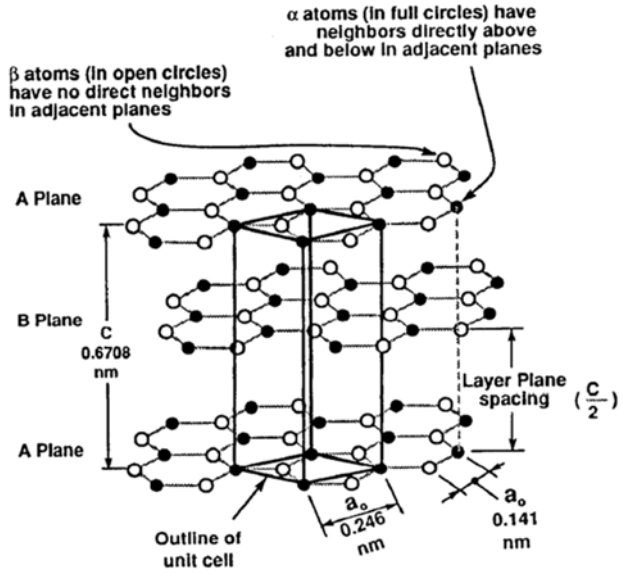

Figure 6. Crystal structure of graphite showing ABAB stacking sequence and unit cell.

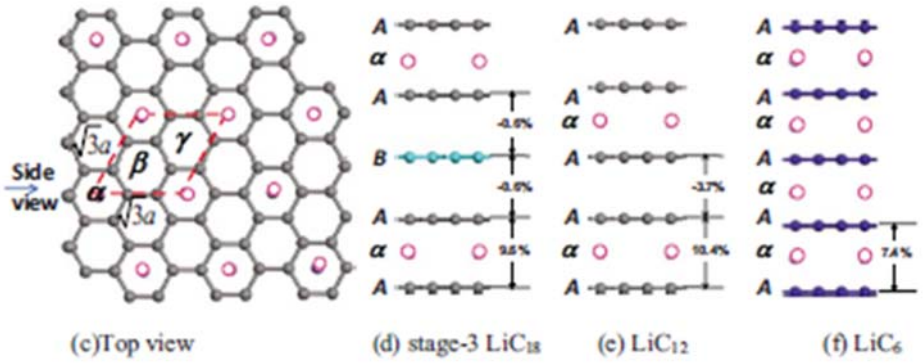

Figure 7. Staging mechanism of Li^+ insertion reaction in graphite.

“staging”, Figure 7.[10]. During this reaction, there are two phase in graphite, so this appeared 3 plateaus in graphite voltage profile.

2.3. Electrolyte

During cell operation, Li^+ is the redox mediator of cathode and anode. When electron flows in external circuit, Li^+ should flow through support electrolyte, because electrical circuit must satisfy the close loop. But, any cation is impossible to be alone in solution without anion. So, Li^+ is dissolved in solution by the form of Li salts. And also, it is necessary to be dissociated well to release Li^+ in electrolyte solution. It needs a certain size of anion, because the more delocalized anion, the more favorable to be dissociated.

To dissociate Li salts better, electrolyte solvents should be high dielectric constant as possible. If it is higher dielectric constant, it can promotes Li salts dissociation. Because the higher dielectric constant decrease coulomb interaction in coulomb force. So, cyclic carbonates are used in electrolyte, they have high dielectric constant. But, cyclic carbonate only showed very high viscosity of solution. Therefore, linear carbonate is mixed to decrease viscosity of electrolyte. If electrolyte is higher viscosity, Li^+ diffusion is unfavorable in electrolyte.

3. Experimental

3.1. Preparation of electrolyte

Bare electrolyte is 1.3 M $LiPF_6$ in EC : EMC : DEC = 3 : 2 : 5. TPFPS(Figure. 3.) was added in this electrolyte by 0.1%, 0.5% weight percent. After adding TPFPS, these mixed electrolytes were stirred overnight. The 0.1 % TPFPS electrolyte was tested in $LiNi_{0.5}Mn_{1.5}O_4$ positive electrode half cell and the 0.5 % electrolyte was tested in graphite *vs.* Li half cell. The electrochemical experiment results was compared with additive-free electrolyte, 1.3 M $LiPF_6$ in EC : EMC : DEC = 3 : 2 : 5.

3.2. Electrode preparation

3.2.1. $LiNi_{0.5}Mn_{1.5}O_4$

$LiNi_{0.5}Mn_{1.5}O_4$ was synthesized by TANAKA of Japan. It is typical spinel structure (Figure 8.) and its particle size is 3~4㎛. $LiNi_{0.5}Mn_{1.5}O_4$ powder was mixed with Super-P. This mixture was dissolved in NMP(N-methyl-2-pyrrolidone) with PVdF(Polyvinyledene fluoride) binder. $LiNi_{0.5}Mn_{1.5}O_4$: Super-P : PVdF was mixed by 94 : 3 : 3 ratio. After that, this slurry was loaded on Al current collector and this electrode foil was heated in 120 ℃ overnight.

3.2.2. Natural graphite

Natural graphite was used as anode material. Its shape is not ideal sphere, surface is a little rough and it particle size is 10~12㎛(Figure 9.). Natural graphite was mixed with Super-P. This mixture was dissolved in NMP(N-methyl-2-pyrrolidone) with PVdF(Polyvinyledene fluoride) binder. Graphite : Super-P : PVdF was mixed by 90 : 5 : 5 ratio. After that, this slurry was loaded on Cu current collector and this electrode foil was heated in 120 ℃ overnight.

3.3. Electrochemical analysis

Electrochemical charge, discharge test was progressed in $LiNi_{0.5}Mn_{1.5}O_4$ electrode and graphite electrode separately. So, coin cell was assembled in the form of $LiNi_{0.5}Mn_{1.5}O_4$ vs. Li and graphite vs. Li half cell each.

Prior to cycle performance and coulombic efficiency test, film or SEI forming step was done in advance. 0.1*C* (12 mA / g) charge / discharge was done once, 0.2 *C* (24 mA / g) charge / discharge was twice and CV charging in 0.05*C* (6 mA / g) scale was done every step. Charge rate of $LiNi_{0.5}Mn_{1.5}O_4$ cell was 0.5 *C* (60 mA / g), 0.05*C* (6 mA / g) CV charging and discharge rate of it was 0.5 *C* (60 mA / g).

SEI forming step was applied to graphite cell equally. 0.1*C* (37.2 mA / g) charge / discharge was once, 0.2 *C* (74.4 mA / g)charge / discharge was twice and CV charging in 0.05*C* (18.6 mA / g) scale was done every step. Charge rate of graphite cell was

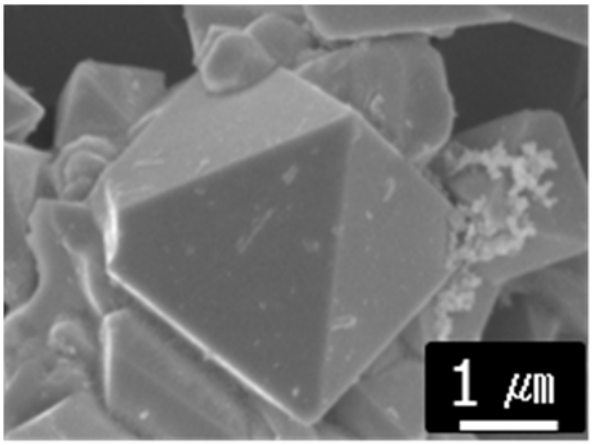

Figure 8. FE-SEM image of $LiNi_{0.5}Mn_{1.5}O_4$ electrode was experimented

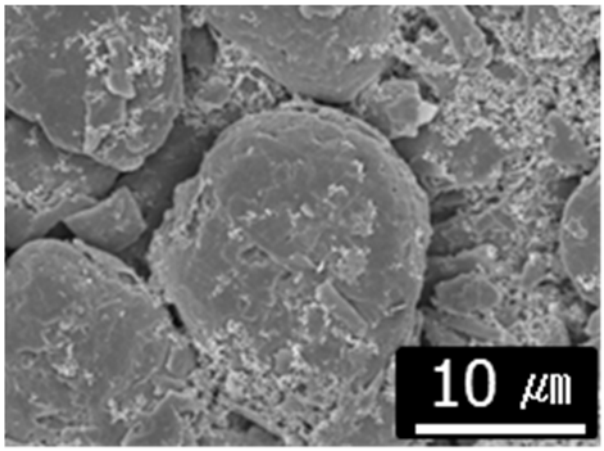

Figure 9. FE-SEM image of natural graphite electrode was experimented

0.5 *C* (186 mA / g), 0.05*C* (18.6 mA / g) CV charging and discharge rate of it was 0.5 *C* (186 mA / g).

Charge / discharge cycler equipment was Wonatech. A. C. Impedance was measured by CHI instruments. Frequency region of impedance was that the minimum was 0.005 Hz and the maximum was 100,000 Hz. The measured electrode was in charged state(~4.7V).

3.4. Spectroscopic analysis

Electrode surface was analyzed by FE-SEM(Field Emission – Scanning Electron Microscope), HR-TEM(High Resolution – Transmission Electron Microscopy), and XPS(X-ray Photoelectron Spectroscopy). The cycled cells were dismantled in an Ar-filled glove box, the cycled electrodes were washed with DEC(Diethylcarbonate). After drying electrodes, they are sealed in 5ml vial, and they were transferred from glove box to instrument chamber.

FE-SEM(JEOL, JSM-6700F) image was collected in 5kV acceleration voltage. HR-TEM(JEOL, JEM-2100F) image was got in 200kV acceleration voltage. The XPS data was collected in ultra-high vacuum multipurpose surface analyze system (Sigma probe, Thermo, UK) , its pressure is $< 10^{-10}$ mbar. The X-ray photoelectrons were excited by Al Kα (1486.6 eV) radiation at a constant power of 150 W (15 kV and 10 mA) ; X-ray spot size 400 μm^2. During data collection, a constant-analyzer-energy mode was used

at a pass energy of 30 eV and a step of 0.1 eV. Atomic percent is relative ratio of the selected elements between them, and it was calculated through XPS data by using atomic sensitivity factor[11]. The measured electrode was in charged state of electrode(~4.7V). XPS was fitted on the basis of hydrocarbon(-CH_2), its binding energy 285.0 eV.

4. Results and discussion

4.1. Additive effects on $LiNi_{0.5}Mn_{1.5}O_4$

4.1.1. Cycle life and coulombic efficiency

$LiMn_2O_4$ failure mechanism during cycling has been known that metal dissolution like Mn^{3+} ion into electrolyte solution is main problem[12]. Dissolved Mn^{3+} ion could decrease $LiMn_2O_4$, and attack on SEI of negative electrode. But, higher voltage material, $LiNi_{0.5}Mn_{1.5}O_4$ failure mechanism was proposed that the electrolyte, polymeric binder, conductive carbon, aluminum current collector, and active material itself are not stable against oxidation, it is much worse in high temperature[13-15].

Among oxidation instability of cell components, electrolyte oxidation is one factor of $LiNi_{0.5}Mn_{1.5}O_4$ capacity degradation. Electrolyte oxidation is correlated with following that electrolyte itself is decomposed on active material and a small trace amount of HF attack in electrolyte on cathode passivation film and active materials. Even though some electrolyte additives are examined to improve this problem[5, 16-

19], very effective electrolyte additives have not been developed for high voltage cathode materials. And also, means to overcome electrolyte oxidation for $LiNi_{0.5}Mn_{1.5}O_4$ in high temperature have been hardly known, except for LiBOB additive, polyimide, BiOF coating[20-22].

The following Figure 10. is cycle life and coulmobic efficiency of TPFPS electrolyte in $LiNi_{0.5}Mn_{1.5}O_4$ vs. Li half cell. TPFPS electrolyte showed continual coulombic efficiency advantage than additive-free electrolyte even in high temperature. This aspect reflects that TPFPS electrolyte prevents further electrolyte decomposition during cycling. Due to this benefit, cycle life was showed better.

Electrolyte decomposition decrease was confirmed by chronoamperommetry. Figure 11. is chronoamperommetry experiment data. This experiment was progressed following that passivation layer forming was done in 1^{st} charging state, after forming, maintained 4.9V constant voltage , and measured in current drop in this high voltage state. Most Li^+ was extracted in constant current charging step, because the theoretical capacity of $LiNi_{0.5}Mn_{1.5}O_4$ is 147.7 mA h g^{-1}, accumulated capacity was reached at the 148 mA h g^{-1} point in that charging step. Next, the current in 4.9V step would be considered further electrolyte decomposition in high voltage atmosphere, less current scale of TPFPS electrolyte means further electrolyte decomposition could be prevented by the film layer, affected by TPFPS electrolyte.

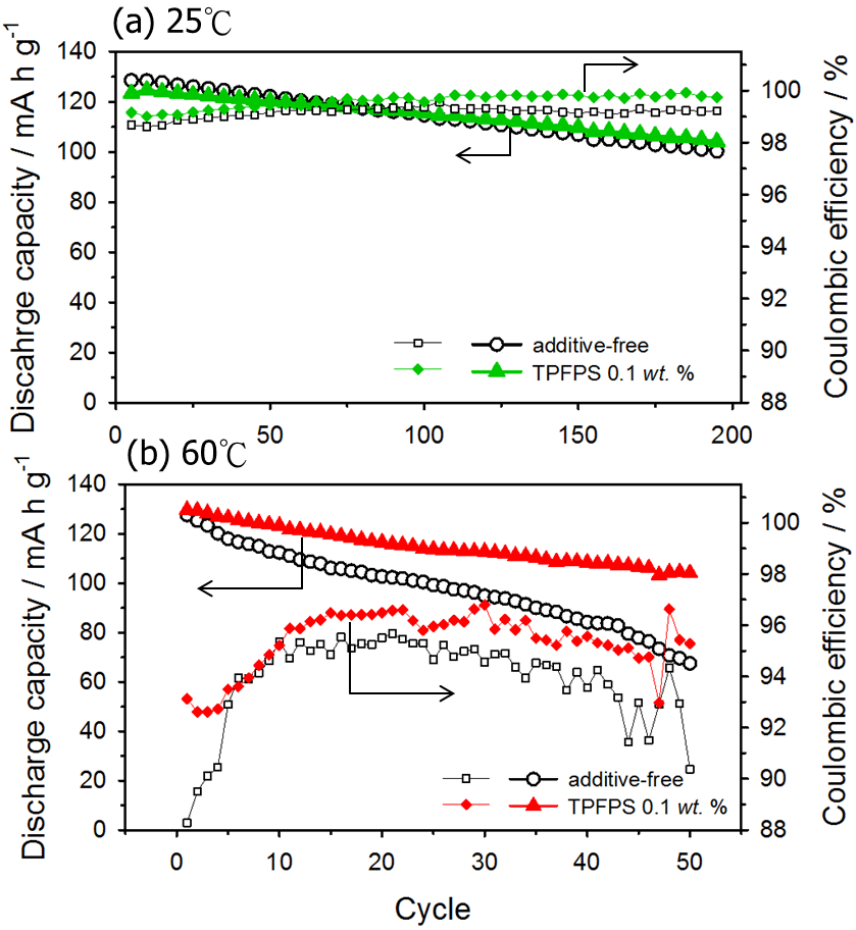

Figure 10. Cycle life and coulombic efficiency of $LiNi_{0.5}Mn_{1.5}O_4$ / Li half cell, showed by TPFPS and additive-free electrolytes. Current density is 0.5 *C*(60 mA/g) *c*-rate and 0.05 *C*(6mA / g) current cut-off CV charging. (a) at 25℃, (b) at 60℃.

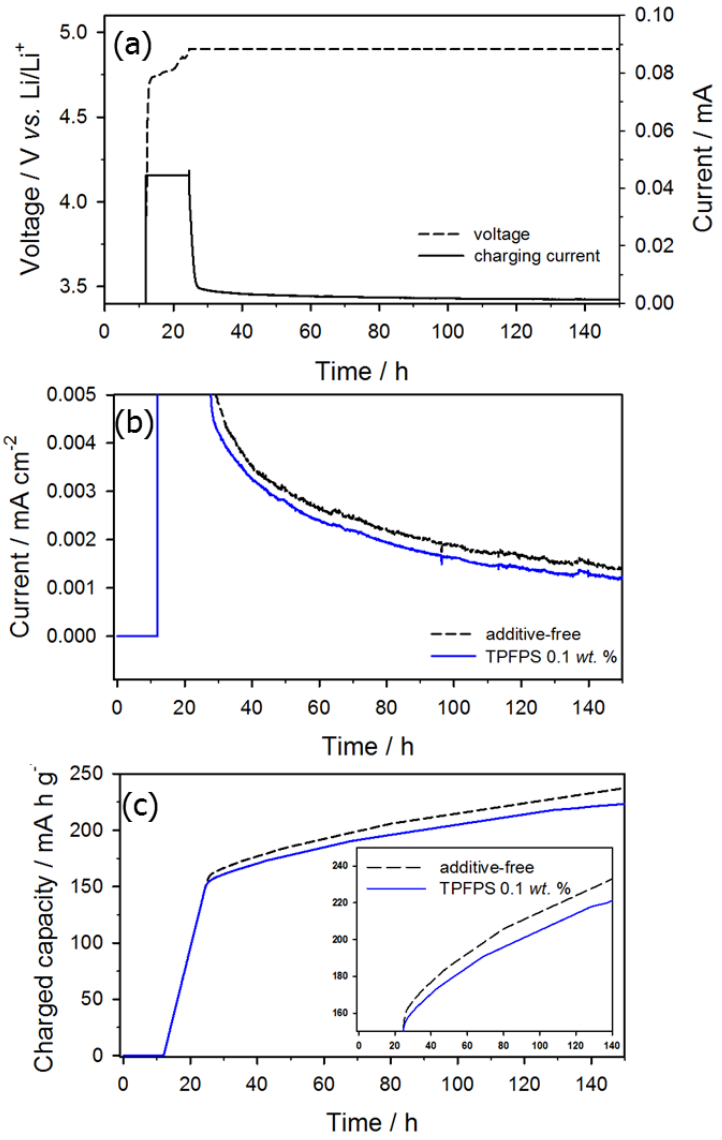

Figure 11. Chronoamperommetry experiment. (a) 1st charging step 0.1*C* (6 mA/g) and maintaining 4.9 V constant voltage. (b) Current drop comparison between additive-free and TPFPS electrolyte during 4.9 V step. (c) The accumulated capacity difference during 4.9V step.

4.1.2. TPFPS reaction aspects on $LiNi_{0.5}Mn_{1.5}O_4$

It is need to consider how TPFPS electrolyte influences on $LiNi_{0.5}Mn_{1.5}O_4$. Figure 12. (a) is differential capacity curve about $LiNi_{0.5}Mn_{1.5}O_4$ *vs.* Li half cell during 1st constant current charging. TPFPS electrolyte induced additional currents in more than 4.4 V(*vs.* Li/Li^+) region. More excess additive quantity showed additional current higher in that region. And Figure 12. (b). showed different capacity plot of 2nd charging step. It showed that more additive quantity, larger overpotential of Li^+ reaction voltage in more than 4.7V region. It means that TPFPS is associated with film forming on $LiNi_{0.5}Mn_{1.5}O_4$ in initial forming stage.

This correlation between film forming and TPFPS additive was confirmed by electrochemical impedance spectroscopy, also. Before explaining impedance plot, cathode impedance equivalent circuit was proposed by M. D. Levi[23]. According to his report, 1st semi-circle is film resistance on cathode materials. And it was analyzed through cathode symmetric cell to exclude Li metal anode resistance effect[24]. These facts are well known to Li-ion battery research.

Figure 13. showed different film resistance between additive-free electrolyte and TPFPS electrolyte. This plot showed TPFPS electrolyte more resistive film on $LiNi_{0.5}Mn_{1.5}O_4$ after 1st charging step. It means that TPFPS affected film forming on $LiNi_{0.5}Mn_{1.5}O_4$ in initial cycling.

And also, it was observed that the more added TPFPS, the thicker film forming on $LiNi_{0.5}Mn_{1.5}O_4$ after 1st cycling by HR-TEM image (Figure 14.). TPFPS electrolyte

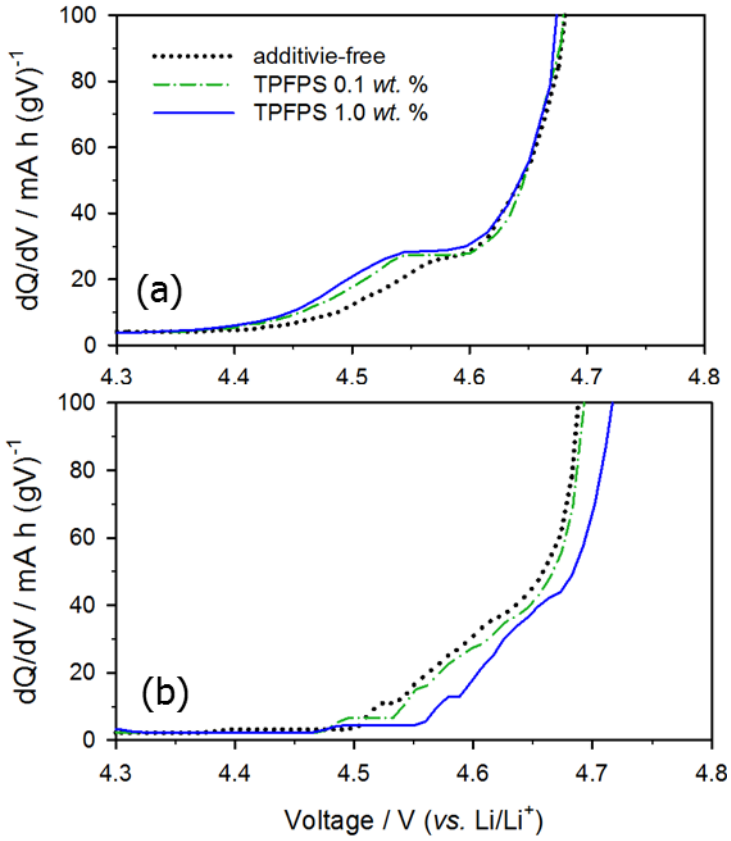

Figure 12. Differential capacity curve during constant current charging on $LiNi_{0.5}Mn_{1.5}O_4$. (a) 1st charging step and (b) 2nd charging step.

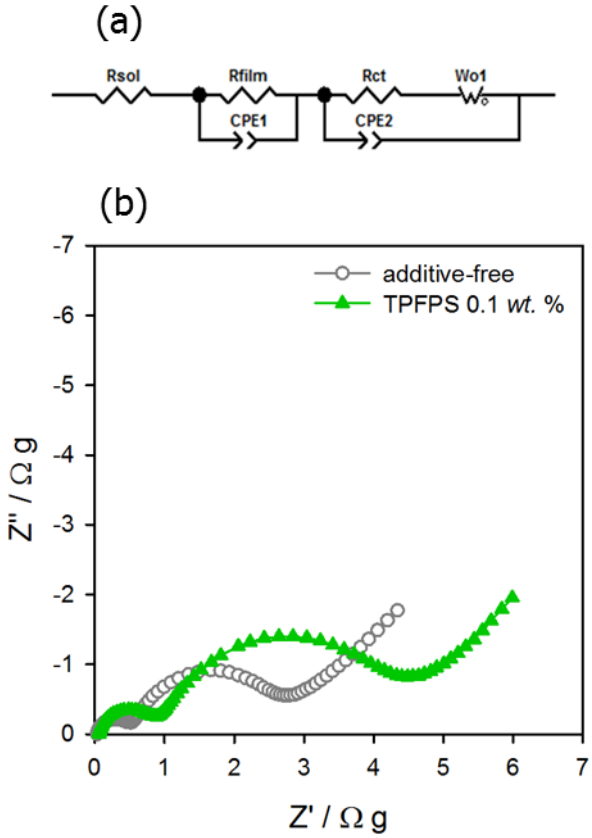

Figure 13. Electrochemical impedance analysis after 1st charging. (a) Equivalent circuit of cathode surface film for fitting and (b) EIS data of $LiNi_{0.5}Mn_{1.5}O_4$ *vs.* $LiNi_{0.5}Mn_{1.5}O_4$ symmetric cell was collected in ~4.73V (*vs.* Li/Li^+), 1st charged state.

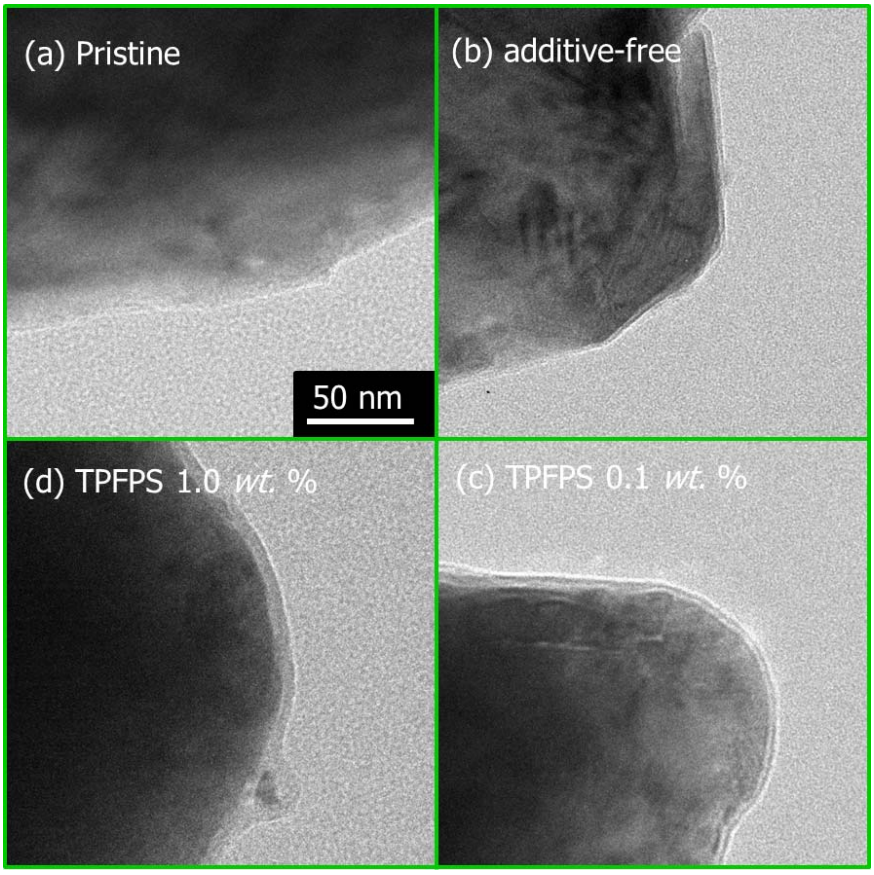

Figure 14. HR-TEM image was collected in 1st charged state. (a) pristine electrode, (b) additive-free, (c) added 0.1 *wt.* % TPFPS and (d) added excess, TPFPS 1.0 *wt.* %.

affects initial film forming on $LiNi_{0.5}Mn_{1.5}O_4$ by considering totally differential capacity curve, electrochemical impedance analysis, HR-TEM.

4.1.3. Comparison of resistance

First, it was searched by voltage profile to confirm how the initial formed film on $LiNi_{0.5}Mn_{1.5}O_4$ affects cycle performance. Figure 15. is voltage profile after cycling. After 1st cycle, TPFPS electrolyte is seemed that less discharge capacity than additive-free electrolyte due to higher resistance of the film layer affected by TPFPS. During cycling, previous mentioned, TPFPS electrolyte showed higher coulombic efficiency, it is due to less electrolyte decomposition in oxidation atmosphere. So, electrolyte decomposed products would be accumulated much less than additive-free electrolyte. This caused far higher polarization, Li^+ reaction voltage gap(~4.7V vs. Li/Li^+) between charge and discharge process after cycling.

Polarization means increasing of electrode resistance. Figure 16. is impedance data of initial and after cycled $LiNi_{0.5}Mn_{1.5}O_4$ electrode. It was much higher that film resistance increase of additive-free electrolyte was than TPFPS electrolyte. Therefore, decomposed electrolyte products of additive-free electrolyte was accumulated much larger than TPFPS electrolyte.

This result was confirmed by FE-SEM image (Figure 17~18.), also. FE-SEM image confirmed that accumulated electrolyte decomposition products of additive-free electrolyte are much larger than TPFPS electrolyte, once again. In considering these

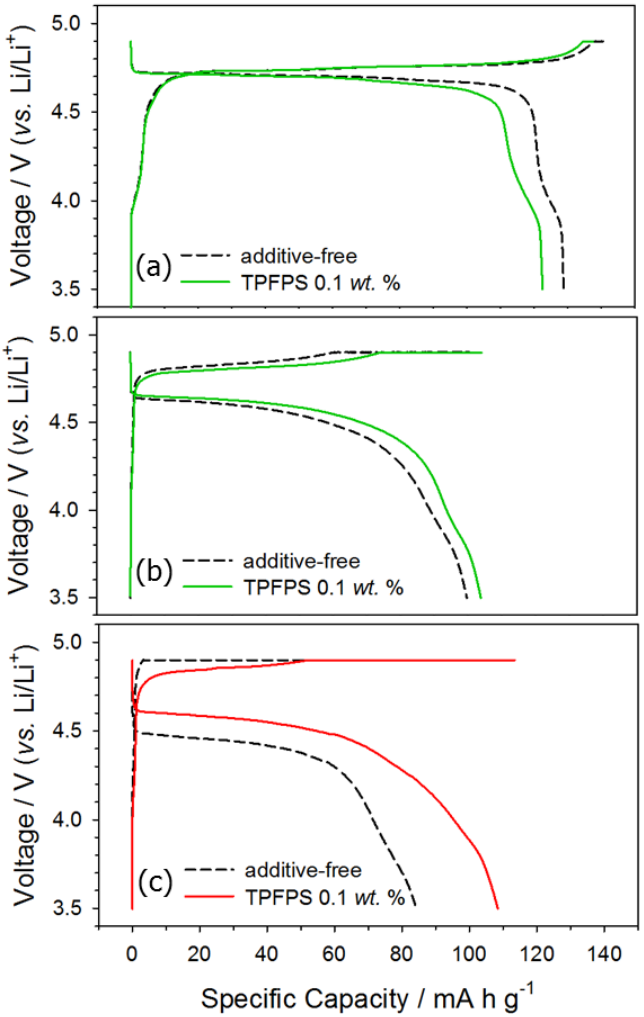

Figure 15. Charge, discharge voltage profiles of $LiNi_{0.5}Mn_{1.5}O_4$ / Li half cell during cycling. (a) Voltage profile of 1st charge, discharge step, (b) 200th voltage profile comparison with additive-free electrolyte and TPFPS electrolyte at 25℃, and (c) 40th voltage profile comparison between them at 60℃.

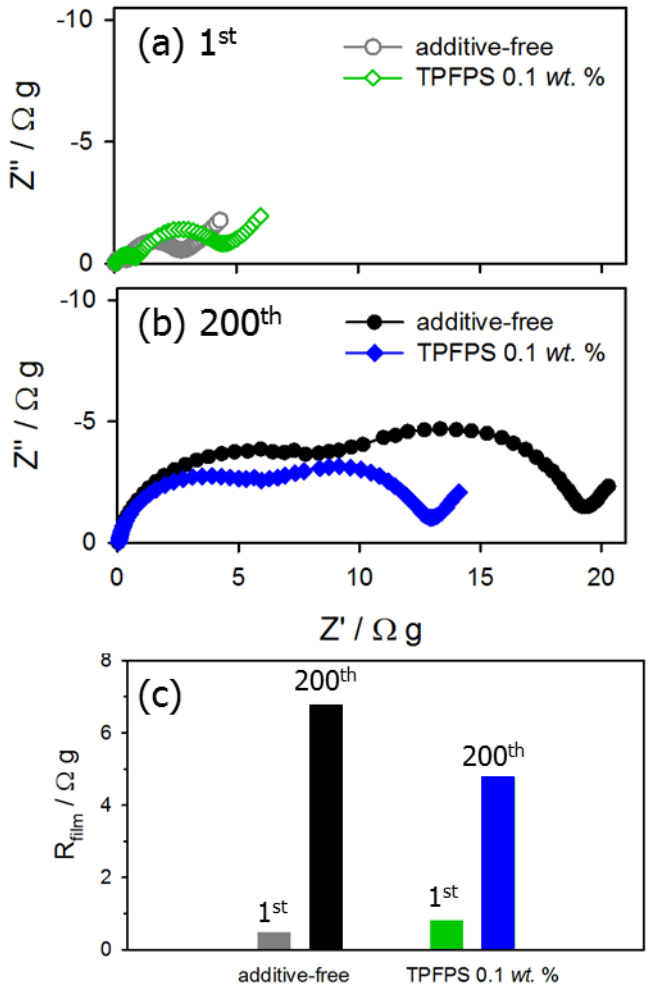

Figure 16. Electrochemical impedance analysis of $LiNi_{0.5}Mn_{1.5}O_4$ *vs.* $LiNi_{0.5}Mn_{1.5}O_4$ symmetric cell before and after cycling. (a) $LiNi_{0.5}Mn_{1.5}O_4$ *vs.* $LiNi_{0.5}Mn_{1.5}O_4$ symmetric cell in 4.73V, 1st charged state (b) $LiNi_{0.5}Mn_{1.5}O_4$ *vs.* $LiNi_{0.5}Mn_{1.5}O_4$ symmetric cell in 4.7V, 200th charged state. (c) Film resistance increase was mitigated in TPFPS electrolyte than additive-free.

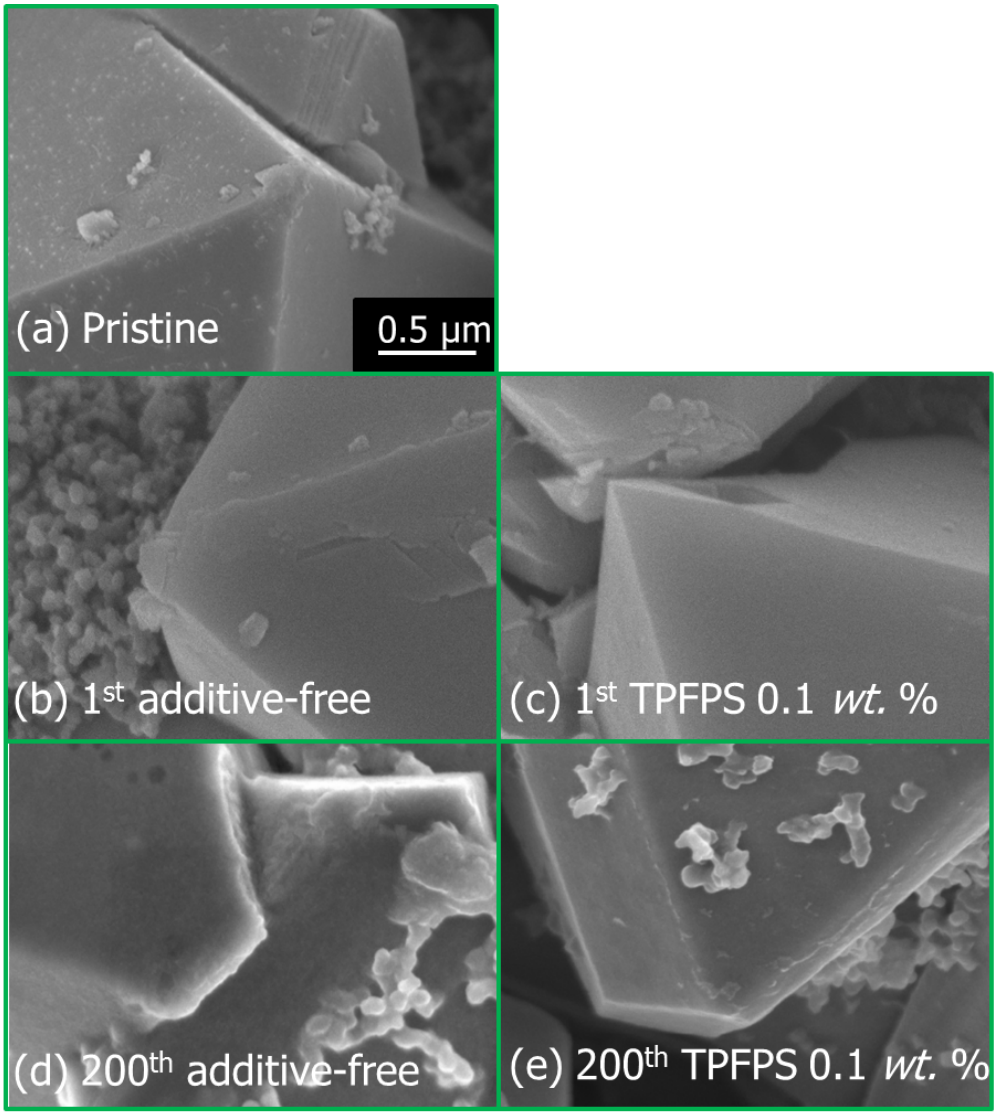

Figure 17. FE-SEM images were collected from pre-cycled electrodes to cycled $LiNi_{0.5}Mn_{1.5}O_4$ electrodes in 25 ℃. (a) Pristine electrode, (b) 1st cycled electrode of additive-free electrolyte, (c) 1st cycled electrode of TPFPS 0.1 *wt.* %, (d) 200th cycled electrode of additive-free, and (e) 200th cycled electrode of TPFPS 0.1*wt.* %.

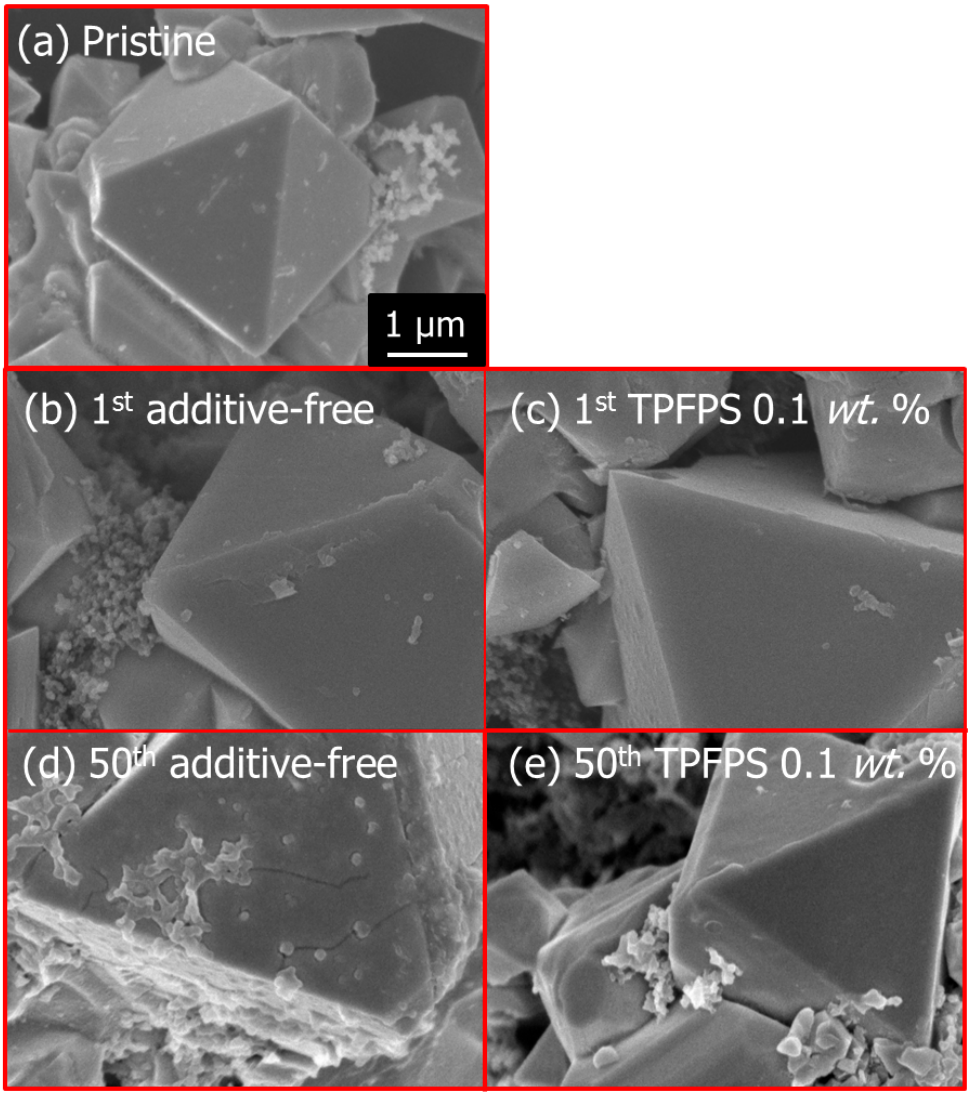

Figure 18. FE-SEM images were collected from pre-cycled electrodes to cycled $LiNi_{0.5}Mn_{1.5}O_4$ electrodes in 60 ℃. (a) Pristine electrode, (b) 1st cycled electrode of additive-free electrolyte, (c) 1st cycled electrode of TPFPS 0.1 *wt.* %, (d) 50th cycled electrode of additive-free, and (e) 50th cycled electrode of TPFPS 0.1 *wt.* %.

images, electrolyte decomposition products was deposited on conducting agent, Super-P as well as active material. Therefore, these electrolyte decomposed products were the one reason of the internal cell resistance increase and the initial film affected by TPFPS must be a mitigating factor during cycling.

4.1.4. Film thickness analysis

In previous section, it was proposed that electrolyte decomposition products were deposited on $LiNi_{0.5}Mn_{1.5}O_4$ electrode surface during cycling. So, it is need to confirm these aspects through X-ray photoelectron spectroscopy. Some chemical bonds of film components and Ni, Mn, and lattice oxygen bonding are following Table 1.[25, 26].

Figure. 19 ~ 21. are XPS topmost of 1^{st} and 200^{th} cycled $LiNi_{0.5}Mn_{1.5}O_4$. Ni. Mn, lattice oxygen topmost intensity is exhibited in them. Plot (a) and (c) of each figures are topmost intensity in 1^{st} charged state and (b), (d) are topmost intensity in 200^{th} charged state. In 1^{st} charged state, Ni, Mn, lattice oxygen intensity of the electrode by TPFPS electrolyte additive was a little bit lower than additive-free electrolyte. As mentioned earlier about film resistance difference, TPFPS affected initial forming step on $LiNi_{0.5}Mn_{1.5}O_4$, the lower Ni, Mn, lattice O intensity of TPFPS electrolyte is due to thicker film layer by TPFPS. Additive-free electrolyte showed much lower Ni, Mn, lattice O intensity than TPFPS electrolyte after cycling.

Table 1. XPS peak assignment of film components on $LiNi_{0.5}Mn_{1.5}O_4$ electrode

	Assignment	Binding energy (eV)
C 1s	Carbon black	284.4
	-CH_2 (Hydrocarbon)	285.0
	<u>C</u>-O	286.1
	O-<u>C</u>-O / <u>C</u>=O	287.6
	O-<u>C</u>=O	289
	Li_2<u>C</u>O_3	290.3
O 1s	$LiNi_{0.5}Mn_{1.5}$<u>O_4</u>	530.3
	O-C=<u>O</u> / Li_2C<u>O_3</u>	532
	<u>O</u>-C=O / <u>O</u>=P$(OR)_3$	533.5
	Li_xPF_y<u>O_z</u>	534.6
F 1s	LiF	685.1
	Li_xPF_y<u>O</u>$_z$	686.6
	PVdF(-C-<u>F</u>)	688
P 2p	O=<u>P</u>$(OR)_3$	134
	Li_x<u>P</u>F_yO_z	136
Li 1s	<u>Li</u>$Ni_{0.5}Mn_{1.5}O_4$	53
	<u>Li_2</u>CO_3	55.5
	<u>Li</u>F	56
	<u>Li_x</u>PF_yO_z	56.8~57
Ni 2p	Mn Auger	850
	$2P_{3/2}$	855.6 / doublet
	$2P_{3/2}$	861.9 / doublet
	Satellite	860 / doublet
Mn 2p	$2P_{3/2}$	643.3 / doublet

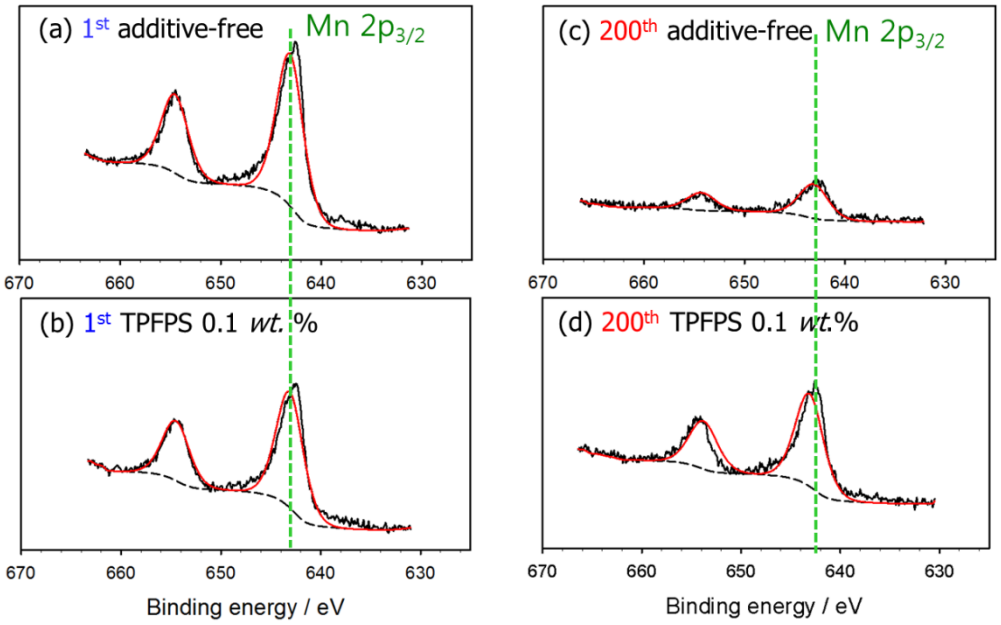

Figure 19. Mn 2p topmost intensity on $LiNi_{0.5}Mn_{1.5}O_4$ electrodes from 1st charged state to 200th charged state. (a) 1st additive-free Mn $2P_{3/2}$ (b) 1st TPFPS (c) 200th additive-free (a) 200th TPFPS.

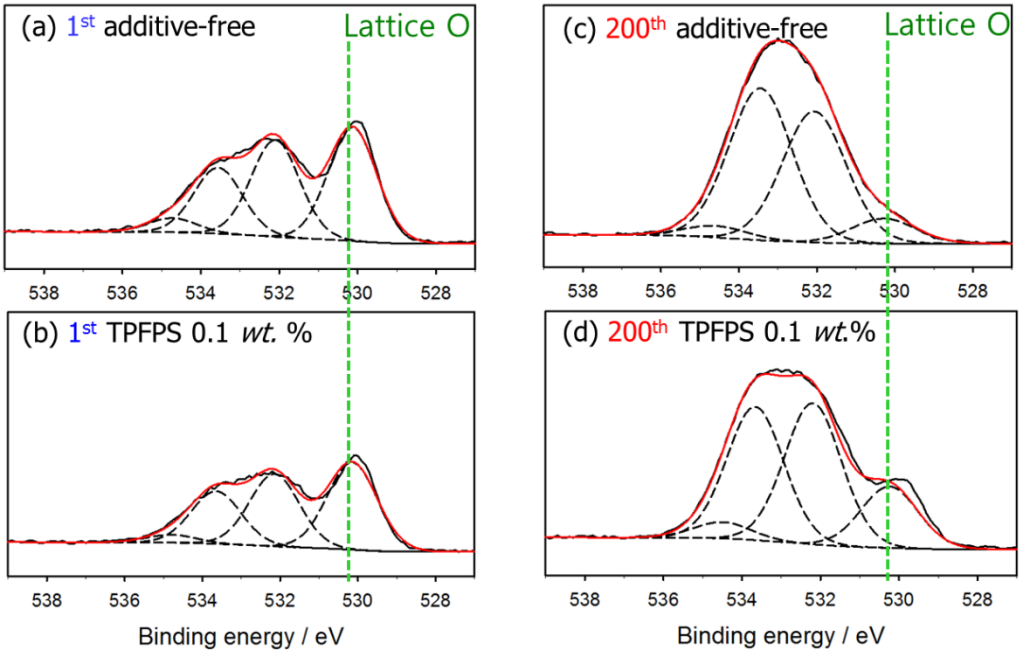

Figure 20. Ni 2p topmost intensity on $LiNi_{0.5}Mn_{1.5}O_4$ electrodes from 1st charged state to 200th charged state. (a) 1st additive-free Mn $2P_{3/2}$ (b) 1st TPFPS (c) 200th additive-free (a) 200th TPFPS.

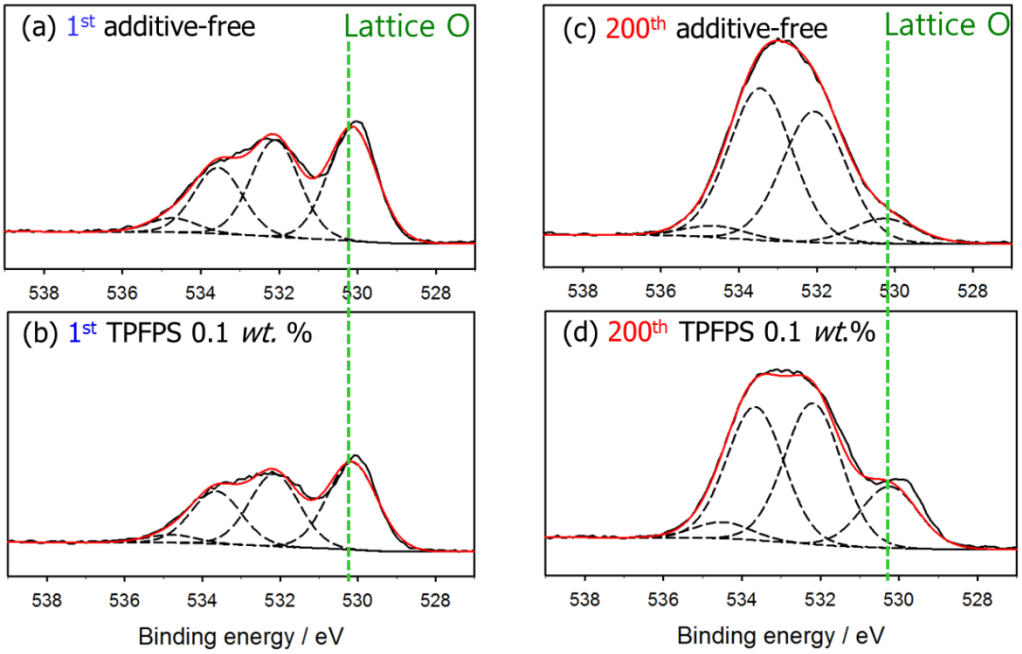

Figure 21. O 1s topmost intensity on $LiNi_{0.5}Mn_{1.5}O_4$ electrodes from 1st charged state to 200th charged state. (a) 1st additive-free Mn $2P_{3/2}$ (b) 1st TPFPS (c) 200th additive-free (a) 200th TPFPS.

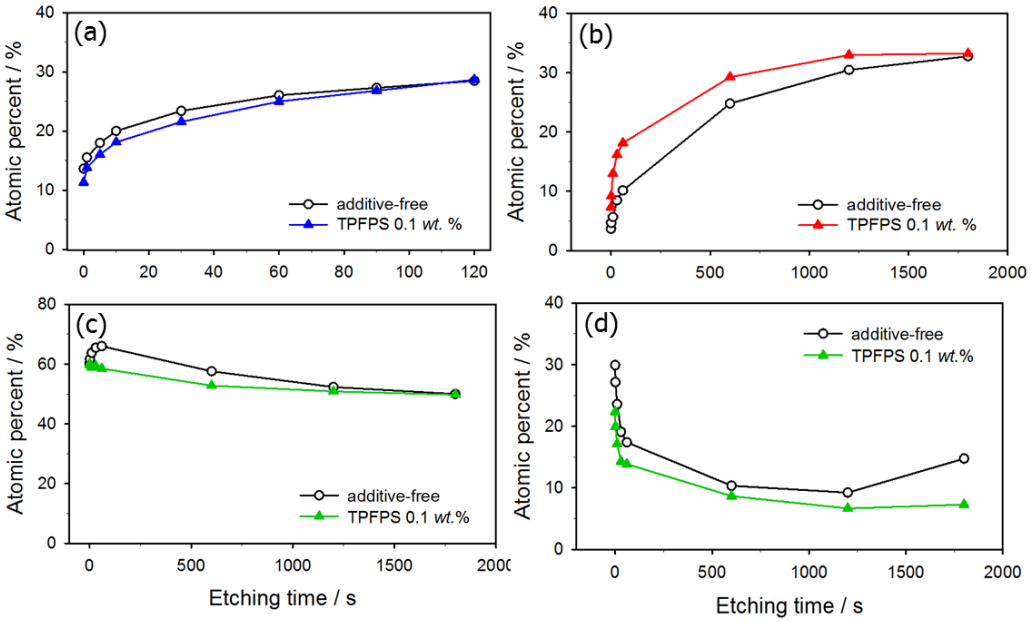

Figure 22. The sum of Ni + Mn + lattice O atomic percent, structure components of $LiNi_{0.5}Mn_{1.5}O_4$, was fitted from XPS depth profiling (a) in 1st charged state, and (b) in 200th charged state (c) total atomic percent of C 1s in 200th charged state (d) O 1s atomic percent derived from electrolyte components.

This means that the passivation layer on $LiNi_{0.5}Mn_{1.5}O_4$ affected by TPFPS had prevented further electrolyte decomposition, compared with additive-free electrolyte, TPFPS had accumulated these detrimental products much less than additive-free.

These aspects were confirmed by XPS depth profiling, Figure. 22. Atomic percent of Ni, Mn, lattice O was more remarkable in TPFPS electrolyte than additive-free electrolyte after cycling. This confirmed that film thickness increase, resulted from electrolyte decomposition, was mitigated by using TPFPS additive. These facts were reflected in C and O except for lattice O atomic percent of depth profiling, Figure 22 (c) and (d). If film is thicker, it would increase the Li^+ diffusion path and contact resistance between active material particles. Therefore, taken together with EIS data, less electrolyte decomposition of TPFPS electrolyte showed less increase of internal cell resistance, the larger capacity during cycling is due to mitigation of internal cell resistance. In conclusion, TPFPS effect is mitigation of film resistance increase during cycling.

4.2. Additive effects on natural graphite

4.2.1. Cycle life and coulombic efficiency

As mentioned earlier(introduction), if we use high voltage merits, low voltage anode materials should be applied with high voltage cathode material in lithium ion battery. The commercialized graphite would be very good partner with $LiNi_{0.5}Mn_{1.5}O_4$.

Graphite / $LiNi_{0.5}Mn_{1.5}O_4$ combination enables an energy density increase when compared with the commercialized cathode materials[27].

Therefore, even though additives for high voltage cathode materials are developed, it would be useless, if these additives can cause harmful effects on anode. For example, VC shows very good performance on anode like graphite, but it could not be applied to graphite / $LiNi_{0.5}Mn_{1.5}O_4$ cell anymore, because of oxidative instability on $LiNi_{0.5}Mn_{1.5}O_4$[4]. So, we must considerate additive effects on the opposite electrode at additive development stage. So, TPFPS was examined in graphite *vs.* Li half cell.

Figure 23. is cycle life and coulmobic efficiency of TPFPS electrolyte in graphite *vs.* Li half cell. TPFPS electrolyte showed continual coulombic efficiency merits than additive-free electrolyte. This reflects that TPFPS electrolyte prevents further electrolyte decomposition during cycling.

4.2.2. TPFPS reaction aspects on Graphite

It is necessary to considerate how TPFPS electrolyte influences on graphite electrode. Figure 24 (a). is differential capacity curve about graphite *vs.* Li half cell during 1st constant current charging. TPFPS begin to be reduced at 1.4 V(*vs.* Li/Li^+) and major sacrificial decomposition would be occurred at around 0.85 V region, 1st peak current. It showed 2nd peak current at around 0.75 V, also. It seems that a little of EC reduction reaction would be occurred earlier than conventional EC reduction peak at 0.7 V. And

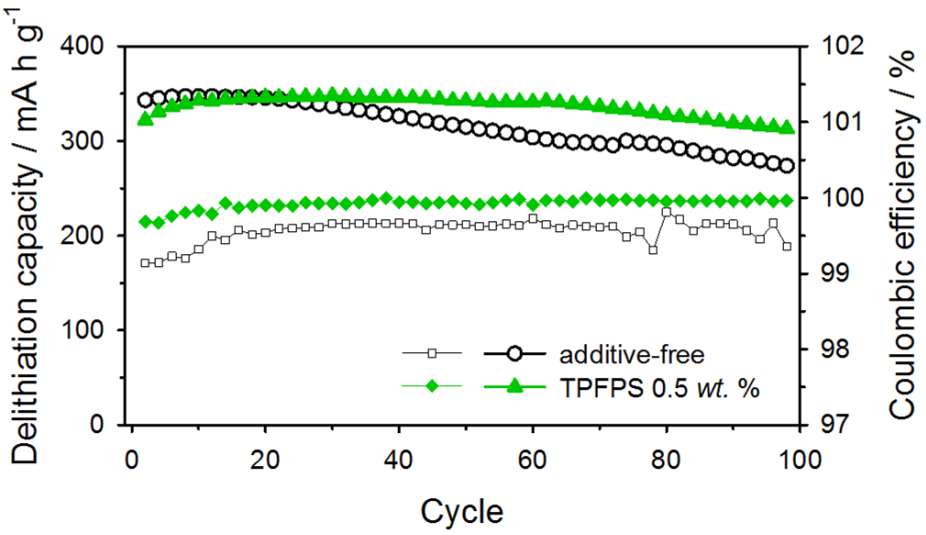

Figure 23. Cycle life and coulombic efficiency of graphite / Li half cell, showed by TPFPS and additive-free electrolytes. Current density is 0.5 *C*(186 mA/g) *c*-rate and 0.05 *C*(18.6 mA/g) current cut-off CV charging.

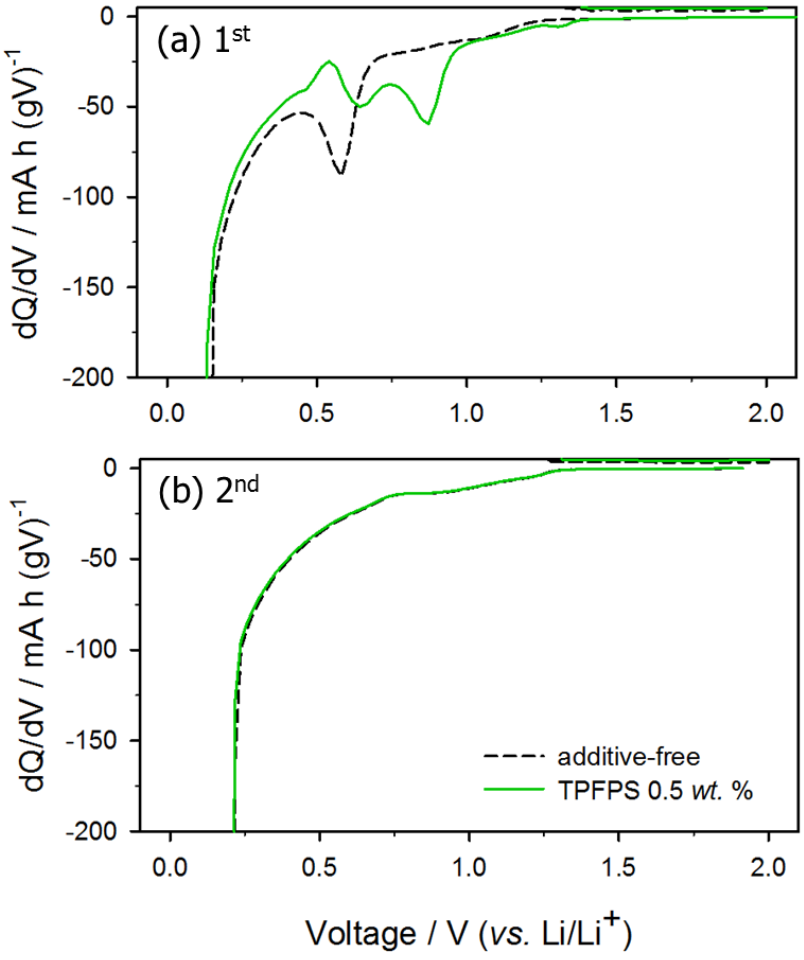

Figure 24. Differential capacity curve during constant current charging on graphite. (a) 1st charging step and (b) 2nd charging step.

Figure 24.(b) showed different capacity plot of 2nd charging step. No additional currents were observed 1.4 V ~ 0.7 V, TPFPS reduction is irreversible and SEI forming reaction.

This correlation between SEI forming and TPFPS additive was confirmed by electrochemical impedance spectroscopy, also. Before explaining impedance plot, graphite electrode impedance equivalent circuit was known[28]. According to this report, 1st semi-circle is SEI resistance on graphite materials. And it was analyzed through graphite symmetric cell to exclude Li metal anode resistance effect[24]. These facts are well known to Li-ion battery research.

Figure 25. showed different film resistance between additive-free electrolyte and TPFPS electrolyte. This plot showed TPFPS electrolyte more resistive SEI on graphite after 1st charging step. It is possible that TPFPS participated in SEI forming on graphite in initial cycling.

XPS data showed more clear that TPFPS itself made different SEI on graphite. Chemical bonds of graphite SEI are following table 2[29-32]. Figure. 26. is XPS data after pre-cycling. Si-C bond was detected in 101 eV[11]. This means that Si-H bond was broken during reduction reaction, tris(pentafluorophenyl)silyl radical anion would be formed. It was clear for TPFPS to be decomposed on graphite sacrificially in 1st charging step. Another important point is LiC_6, 282.6eV lithiated graphite, less intensity of LiC_6 in TPFPS electrolyte is thicker SEI on graphite than additive-free electrolyte.(In fact, this paper said LiC_6 binding energy 282.1 eV, but this difference is.

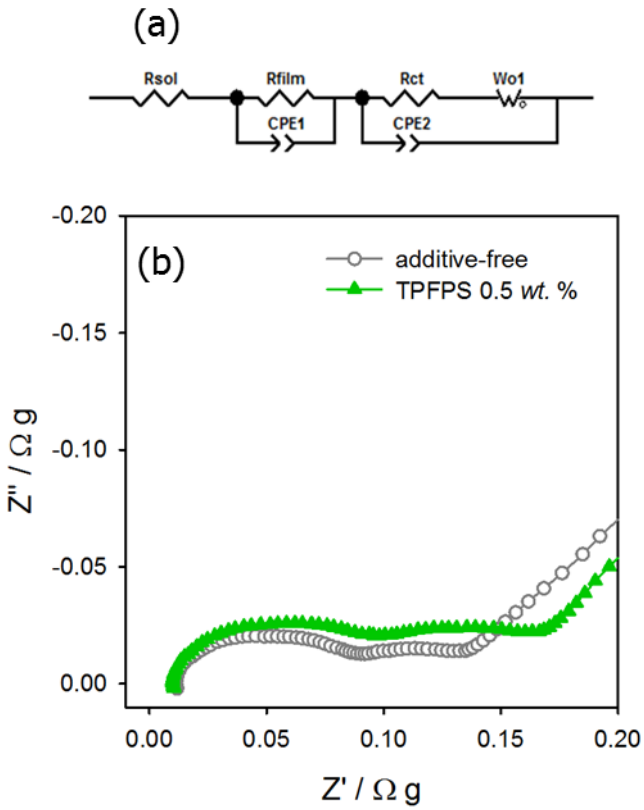

Figure 25. Electrochemical impedance analysis after 1st lithiation. (a) Equivalent circuit of graphite SEI for fitting and (b) EIS data of graphite *vs.* graphite symmetric cell was collected in ~0.88V (*vs.* Li/Li^+) 1st lithiated state.

Table 2. XPS peak assignment of SEI components on graphite electrode

	Assignment	Binding energy (eV)
C 1s	LiC_6	282.6
	Carbon black	284.4
	$-CH_2$ (Hydrocarbon)	285.0
	C-O	286.1
	O-C-O / C=O	287.6
	O-C=O	289
	Li_2CO_3	290.3
O 1s	O-C=O / Li_2CO_3	532
	O-C=O / $O=P(OR)_3$	533.5
	$Li_xPF_yO_z$	534.6
F 1s	LiF	685.0
	$Li_xPF_yO_z$	686.6
	PVdF(-C-F)	688
P 2p	$O=P(OR)_3$	134
	$Li_xPF_yO_z$	136
Li 1s	$LiNi_{0.5}Mn_{1.5}O_4$	53
	Li_2CO_3	55.5
	LiF	56
	$Li_xPF_yO_z$	56.8~57

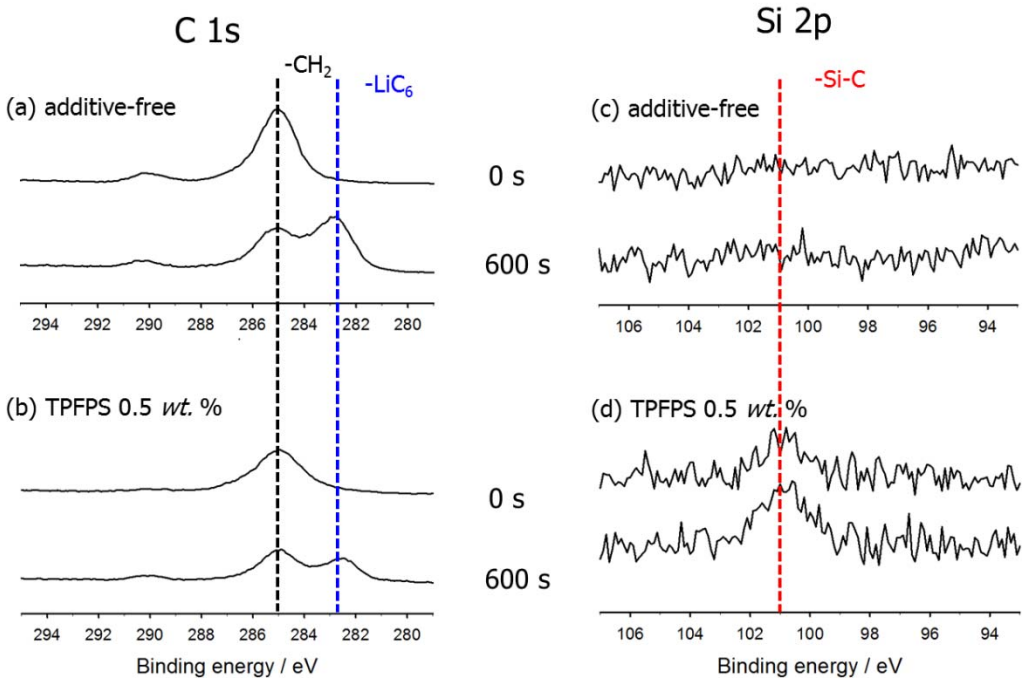

Figure 26. XPS depth profiling was collected from lithiated graphite electrode in pre-cycled step. (a) C 1s spectra of additive-free, (b) Si 2p spectra of additive-free, (c) C 1s spectra of TPFPS 0.5 %, and (d) Si 2p spectra of TPFPS 0.5 %.

resulted from hydrocarbon(-CH_2) charge shift. This paper, hydrocarbon(-CH_2) is 284.5 eV, so 0.5 eV difference is occurred.) Therefore, TPFPS made different SEI on graphite sacrificially by itself in initial step

Figure. 27. is FE-SEM images after 1st lithiation step. First, SEI of additive-free electrolyte had some void region in its surface. On the other hand, SEI formed by TPFPS showed more porous than additive-free electrolyte. Thus, it is clear that TPFPS made different SEI on graphite in 1st lithiation step.

4.2.3. Comparison of resistance

Electrochemical impedance data was following Figure. 28. This plot shows it was mitigated to increase SEI resistance increase of TPFPS electrolyte, when compared with additive-free electrolyte. As mentioned earlier in previous section , because the formed SEI by TPFPS showed higher coulombic efficiency, further electrolyte decomposition was less. So, electrolyte decomposition products had been less decomposed in TPFPS electrolyte. It was confirmed by less increase of SEI resistance than additive-free electrolyte.

4.2.4. Comparison of SEI components

According to EIS data, there is need to examine how resistance merit could be occurred in TPFPS electrolyte during cycling. It seems to be difficult to analyze SEI thickness like film thickness analysis on $LiNi_{0.5}Mn_{1.5}O_4$. Because it was known that

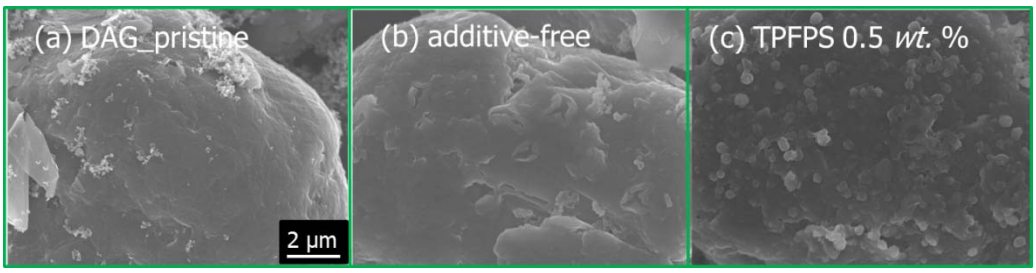

Figure 27. FE-SEM images were obtained from 1st lithiation step. (a) pristine electrode, (b) SEI formed by additive-free electrolyte, and (c) SEI formed by TPFPS.

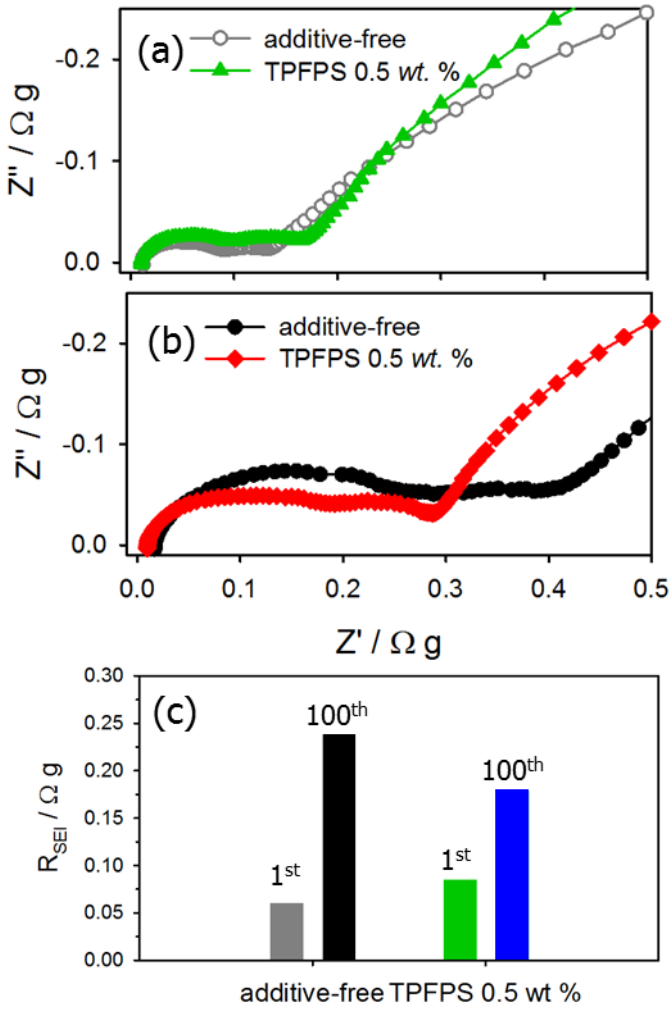

Figure 28. Electrochemical impedance analysis of graphite *vs.* graphite symmetric cell before and after cycling. (a) Graphite *vs.* graphite symmetric cell in 0.088V, 1st lithiated state (b) Graphite *vs.* graphite symmetric cell in 0.2V, 100th lithiated state. (c) SEI resistance increase was mitigated in TPFPS electrolyte than additive-free.

SEI is much thicker than cathode film, and the peaks of carbon, component of carbon, is very broad when compared with other atom elements. So, it should be analyzed differently unlike cathode film. Another approach is to survey SEI components on graphite.

Before explaining the results, there is necessary to know correlation between SEI components and SEI resistance. First, SEI model on graphite has been established to some degree through some papers[33-35]. These papers said that inorganic components is in topmost of graphite surface, organic components is in upper layer than inorganic components. So, SEI components is classified into organic parts and inorganic parts. But, it is wondered what components are more resistive than others from the point of Li^+ diffusion.

These questions are solved to some extent through these papers[36, 37]. They conducted isotope exchange experiments. Mass of SEI forming elements and mass of soaking elements were different. In their experiments, they revealed that Li^+ diffusion is very fast in organic phase than inorganic phase, and Li^+ can pass into organic layer in solvation state with salt anion. But, in inorganic phase, salt anion can’t go through this layer, and there was a saturation point that Li^+ isotope exchange can’t be occurred fast. This means that Li^+ diffusion is unfavorable in inorganic phase than organic phase. So, the richer inorganic components in SEI, the more resistive electrode from the point of Li^+ diffusion ,as a result.

In view of these points, it could be said that inorganic constituents are more resistive SEI. It has been known that Li_2O, Li_2CO_3, LiF are certainly inorganic components[33-37]. Figure 29. are XPS depth profiling, collected after 100^{th} cycled, charged state. Clarification between Li_2CO_3 and LiOH is difficult, because their binding energy is very adjacent, 531.6 eV and 532 eV each. So, intensity of Li_2O and LiF only was analyzed. Li_2O, of which binding energy is 528.8eV[31], and LiF[32], its binding energy is 685.0eV were much richer in additive-free than TPFPS electrolyte. It was confirmed more clearly by atomic percent of depth profiling, Figure 30. Because inorganic species like Li_2O and LiF has being abundant in additive-free electrolyte during cycling, SEI resistance increase must not have mitigated than TPFPS electrolyte.

Furthermore, these inorganic components are known to electrical insulator[38, 39], because their band gap higher than 1.5 eV[40]. And when these components were accumulated on conducting agent and polymeric binder, contact resistance between active materials would be much higher. Therefore, less electrode resistance increasing by TPFPS electrolyte is due to less accumulation of inorganic species like Li_2O and LiF.

These richer components of SEI in additive-free electrolyte are confirmed by FE-SEM images(Figure 31.). As mentioned earlier, inorganic species are known to more dense layer than organic components[33]. Additive-free electrolyte showed more dense layer. On the other hand, TPFPS electrolyte has more porous layers after cycling.

Therefore, considering higher columbic efficiency of TPFPS, electrolyte decomposition aspects were different during cycling, SEI of TPFPS electrolyte has

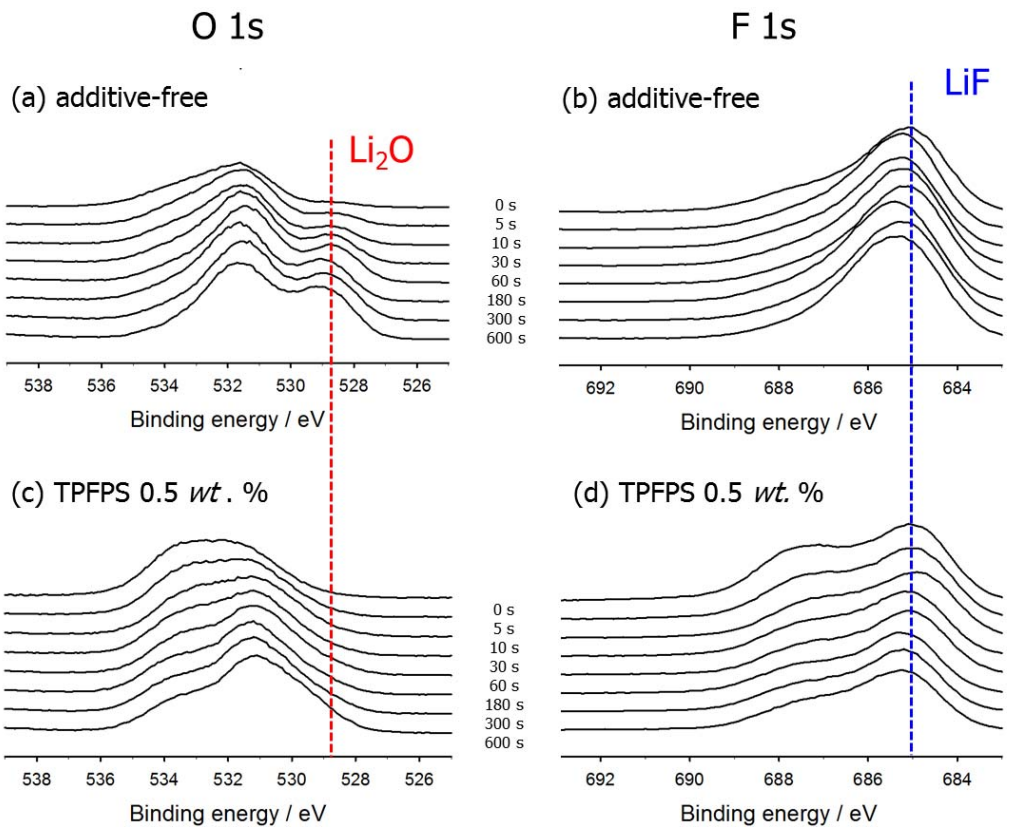

Figure 29. O 1s and F XPS depth profile of 100th lithiated graphite electrodes. (a) O 1s spectra of additive-free electrolyte, (b) F 1s spectra of additive-free electrolyte, (c) O 1s spectra of TPFPS 0.5 *wt.* %, and (d) F 1s spectra of TPFPS 0.5 *wt.* %.

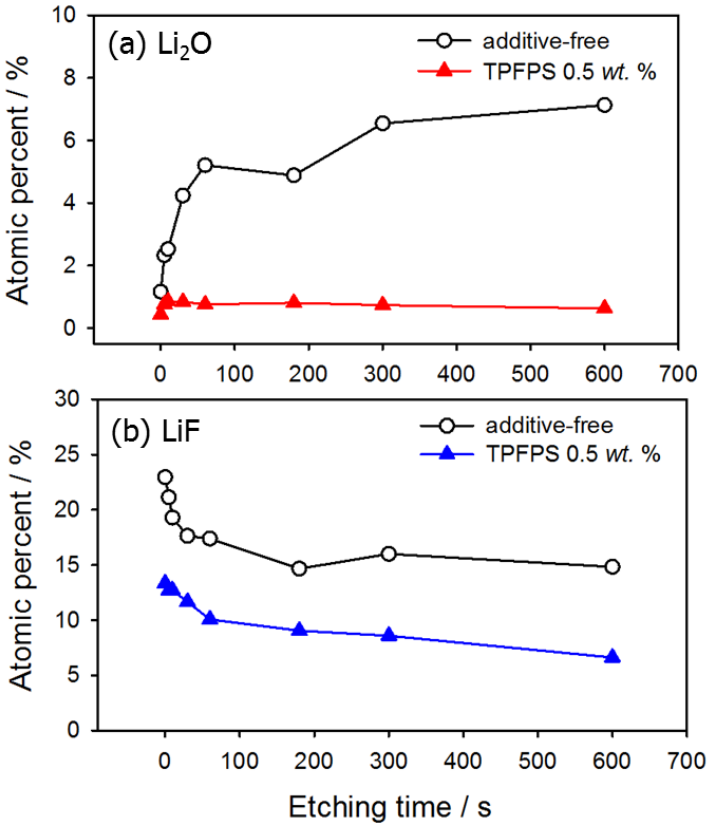

Figure 30. Li_2O and LiF atomic percent of XPS depth profiling. (a) Li_2O component on graphite, and (b) LiF component on graphite.

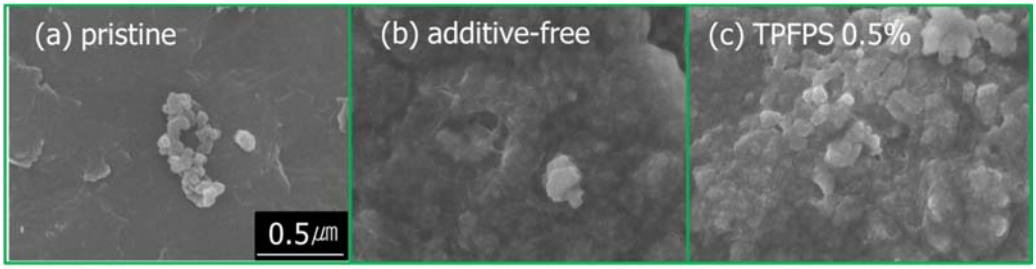

Figure 31. FE-SEM images were obtained from 100th lithiation step. (a) pristine electrode, (b) SEI of additive-free electrolyte, and (c) SEI of TPFPS after cycling.

being accumulated to less inorganic species. This is the reason that SEI resistance mitigation could be occurred in TPFPS electrolyte. This resistance advantage during cycling is possible to make cycle life much longer.

5. Conclusion

$LiNi_{0.5}Mn_{1.5}O_4$ and graphite electrodes operate beyond electrochemical stability window of electrolyte[1]. These side reactions appear continually during cycling because of not reach to 100% coulombic efficiency and accumulated film or SEI resistance would be one reason of cell degradation. TPFPS additive could improve this problem and this additive showed good cycle life on both positive and negative electrodes.

In both electrodes, TPFPS additive could mitigate internal cell resistance attributed to electrolyte decomposition in oxidation and reductive atmosphere. This was confirmed through film thickness in case of $LiNi_{0.5}Mn_{1.5}O_4$ and less inorganic components in case of graphite electrode. In conclusion, TPFPS could mitigate film resistance increase on both each electrodes, because it reduce electrolyte decomposition during cycling.

References

[1] J.B. Goodenough, Y. Kim, Journal of Power Sources, 196 (2011) 6688-6694.
[2] E. Peled, Journal of The Electrochemical Society, 126 (1979) 2047-2051.
[3] S. Park, J. Heon Ryu, S.M. Oh, Journal of The Electrochemical Society, 158 (2011) A498-A503.
[4] H. Lee, S. Choi, S. Choi, H.-J. Kim, Y. Choi, S. Yoon, J.-J. Cho, Electrochemistry Communications, 9 (2007) 801-806.
[5] M. Xu, Y. Liu, B. Li, W. Li, X. Li, S. Hu, Electrochemistry Communications, 18 (2012) 123-126.
[6] G.-B. Han, J.-N. Lee, J.W. Choi, J.-K. Park, Electrochimica Acta, 56 (2011) 8997-9003.
[7] C.M. Julien, A. Mauger, Ionics, 19 (2013) 951-988.
[8] K. Takahashi, M. Saitoh, M. Sano, M. Fujita, K. Kifune, Journal of The Electrochemical Society, 151 (2004) A173-A177.
[9] Hugh O. Pierson, Handbook of carbon, graphite, diamond and fullerens, 1993
[10] Y. Qi, H. Guo, L.G. Hector, A. Timmons, Journal of The Electrochemical Society, 157 (2010) A558-A566.
[11] J. F. Moulder, HAndbook of X-ray Photoelectron Spectroscopy, 1978
[12] D.H. Jang, Y.J. Shin, S.M. Oh, Journal of the Electrochemical Society, 143 (1996) 2204-2211.
[13] T. Yoon, S. Park, J. Mun, J.H. Ryu, W. Choi, Y.-S. Kang, J.-H. Park, S.M. Oh, Journal of Power Sources, 215 (2012) 312-316.
[14] Y. Talyosef, B. Markovsky, G. Salitra, D. Aurbach, H.J. Kim, S. Choi, Journal of Power Sources, 146 (2005) 664-669.
[15] B. Markovsky, Y. Talyossef, G. Salitra, D. Aurbach, H.-J. Kim, S. Choi, Electrochemistry Communications, 6 (2004) 821-826.
[16] Y.-S. Kang, T. Yoon, S.S. Lee, J. Mun, M.S. Park, J.-H. Park, S.-G. Doo, I.-Y. Song, S.M. Oh, Electrochemistry Communications.
[17] V. Tarnopolskiy, J. Kalhoff, M. Nádherná, D. Bresser, L. Picard, F. Fabre, M. Rey, S.

Passerini, Journal of Power Sources, 236 (2013) 39-46.
[18] S. Dalavi, M. Xu, B. Knight, B.L. Lucht, Electrochemical and Solid-State Letters, 15 (2011) A28-A31.
[19] L.Y. Xing, M. Hu, Q. Tang, J.P. Wei, X. Qin, Z. Zhou, Electrochimica Acta, 59 (2012) 172-178.
[20] H.-B. Kang, S.-T. Myung, K. Amine, S.-M. Lee, Y.-K. Sun, Journal of Power Sources, 195 (2010) 2023-2028.
[21] J.-H. Cho, J.-H. Park, M.-H. Lee, H.-K. Song, S.-Y. Lee, Energy & Environmental Science, 5 (2012) 7124-7131.
[22] S.-Y. Ha, J.-G. Han, Y.-M. Song, M.-J. Chun, S.-I. Han, W.-C. Shin, N.-S. Choi, Electrochimica Acta, 104 (2013) 170-177.
[23] M.D. Levi, G. Salitra, B. Markovsky, H. Teller, D. Aurbach, U. Heider, L. Heider, Journal of the Electrochemical Society, 146 (1999) 1279-1289.
[24] C.H. Chen, J. Liu, K. Amine, Journal of Power Sources, 96 (2001) 321-328.
[25] Y.-C. Lu, A.N. Mansour, N. Yabuuchi, Y. Shao-Horn, Chemistry of Materials, 21 (2009) 4408-4424.
[26] S. Ivanova, E. Zhecheva, R. Stoyanova, D. Nihtianova, S. Wegner, P. Tzvetkova, S. Simova, The Journal of Physical Chemistry C, 115 (2011) 25170-25182.
[27] K.W. Leitner, H. Wolf, A. Garsuch, F. Chesneau, M. Schulz-Dobrick, Journal of Power Sources, 244 (2013) 548-551.
[28] C. Wang, A.J. Appleby, F.E. Little, Electrochimica Acta, 46 (2001) 1793-1813.
[29] P. Verma, P. Maire, P. Novák, Electrochimica Acta, 55 (2010) 6332-6341.
[30] P. Niehoff, S. Passerini, M. Winter, Langmuir, 29 (2013) 5806-5816.
[31] K. Kanamura, S. Shiraishi, H. Takezawa, Z.-i. Takehara, Chemistry of Materials, 9 (1997) 1797-1804.
[32] H. Park, T. Yoon, J. Mun, J.H. Ryu, J.J. Kim, S.M. Oh, Journal of The Electrochemical Society, 160 (2013) A1539-A1543.
[33] K. Edström, M. Herstedt, D.P. Abraham, Journal of Power Sources, 153 (2006)

380-384.
[34] K. Xu, A. von Cresce, Journal of Materials Chemistry, 21 (2011) 9849-9864.
[35] K. Xu, Chem. Rev., 104 (2004) 4303-4418.
[36] P. Lu, S.J. Harris, Electrochemistry Communications, 13 (2011) 1035-1037.
[37] S. Shi, P. Lu, Z. Liu, Y. Qi, L.G. Hector, H. Li, S.J. Harris, J. Am. Chem. Soc., 134 (2012) 15476-15487.
[38] A.B. Kunz, Physical Review B, 26 (1982) 2056-2069.
[39] Y. Duan, D.C. Sorescu, Physical Review B, 79 (2009) 014301.
[40] Allen J. Bard, Electrochemical Methods - Fundamnentals and applications 2nd (2001).

요 약(국문초록)

리튬 이차 전지가 상용화된 이래로, IT 모바일 기기에서부터 EV에 이르기 까지 그 수요가 널리 확대되고 있다. 이러한 경향에 따라, 리튬 이차 전지는 더욱 높은 에너지 밀도를 낼 수 있도록 요구되고 있다. 전지의 에너지 밀도를 높일 수 있는 방법은 용량을 증가시키는 방법과 전압을 올리는 방법이 있는데, 많은 연구자들이 전압을 올리는 방법을 많이 시도하고 있다. 더 높은 작동 전압에서 구동하는 전지를 만들려면, 기존의 저전압 음극은 그대로 사용하는 가운데, 양극의 작동 전압을 높여야 한다.

그런데, 고전압 양극을 적용시키기 위해서는 기존의 전해질이 산화되는 문제점에 직면해 있다. 이러한 문제를 해결하기 위해서 가격과 공정상의 이점 때문에 전해액 첨가제를 사용하는 방법이 가장 선호되고 있다. 그런데, 저전압 전극을 위한 첨가제는 많이 개발되어 있으나, 고전압 양극을 위한 첨가제는 아직까지 별로 알려진 것이 없다. 기존에 음극에서 좋은 성능을 보였던 VC같은 첨가제는 고전압 양극에 적용시킬 때, 산화 안정성 때문에 더 이상 사용할 수 없게 되었다.

따라서, 이번 연구는 양극과 음극의 수명을 동시에 향상시키고자 하는 전해액 첨가제의 개발에 관한 것이다. Tris(pentafluorophenyl)silane 첨가제는 양극과 음극의 수명과 효율을 동시에 향상시켜 줄 수 있음을 보여주었다. TPFPS 효과를 한 마디로 요약하자면, 충·방전 과정에서 일어나는 양극과 음극의 저항 증가를 동시에 완화시켜 줄 수 있다는 것이다. 이러한 결과는 XPS data를 통해, 양극의 경우 증가된 $LiNi_{0.5}Mn_{1.5}O_4$ 피막의 두께를 분석함으로써, 음극은 증가된 무기물 성분을 분석함으로써 그 효과를 입증할 수 있었다.